IMPROVING PERFORMANCE AND ROTORDYNAMIC CHARACTERISTICS OF INJECTION COMPRESSORS VIA MUCH LONGER BALANCE-PISTON AND DIVISION-WALL SEALS

A Thesis

by

MARGARITA RODRIGUES RODRIGUES

Submitted to the Office of Graduate Studies of
Texas A&M University
in partial fulfillment of the requirements for the degree of

MASTER OF SCIENCE

December 2006

Major Subject: Mechanical Engineering

IMPROVING PERFORMANCE AND ROTORDYNAMIC CHARACTERISTICS OF INJECTION COMPRESSORS VIA MUCH LONGER BALANCE-PISTON AND DIVISION-WALL SEALS

A Thesis

by

MARGARITA RODRIGUES RODRIGUES

Submitted to the Office of Graduate Studies of
Texas A&M University
in partial fulfillment of the requirements for the degree of

MASTER OF SCIENCE

Approved by:

Chair of Committee, Dara Childs
Committee Members, John Vance
Luciana Barroso
Head of Department, Dennis L. O'Neal

December 2006

Major Subject: Mechanical Engineering

ABSTRACT

Improving Performance and Rotordynamic Characteristics of Injection Compressors via Much Longer Balance-Piston and Division-Wall Seals. (December 2006)
Margarita Rodrigues Rodrigues, B.S., Universidad Simón Bolívar
Chair of Advisory Committee: Dr. Dara W. Childs

Predictions are presented for a selected compressor using longer hole-pattern seals with L/D ratios from 0.5 to 2.5. Results were obtained for back-to-back and in-line compressors with the seal located at mid-span and at 82% of rotor span respectively, considering different seal lengths, radial seal clearances, as well as constant clearance and convergent-tapered seal geometries.

Predictions of the synchronous rotordynamic coefficients and leakage were estimated using a code developed by Kleynhans and Childs with zero preswirl and constant pressure ratio of 0.5. This code does not include moment coefficients; which can affect the results.

Results of all configurations show an increase of stiffness and damping coefficients with increasing seal length. In addition, a significant reduction in leakage (approximately 47 percent) as L/D increases is exhibited for constant clearance and convergent-tapered hole-pattern seals.

For the back-to-back compressor, the stability analysis predicts that the system is stable for all speeds and L/D ratios. In fact, the rotor cylindrical-bending mode becomes more stable with lengthening the seals, for both constant clearance and convergent-tapered hole-pattern seals. For constant clearance seals (Case A), the synchronous response at mid-span show a critical speed at 8,000 rpm (cylindrical-bending mode) for all L/D ratios, while a reduction of 85 percent in the peak response is exhibited as L/D increases. Case B, in which the radial clearance is increased as L/D increases to have the same leakage as case A, slightly increases the synchronous response of the model compared to case A. For convergent-tapered seals (Case C), the synchronous response at mid-span shows a higher critical speed (9,000 rpm) for all L/D ratios, and a larger reduction (89 percent) in peak response with increasing L/D,

compared to Case A. However, the magnitude of the peak response is larger for convergent-tapered seals than that for constant clearance seals, for all L/D ratios.

For in-line compressor, the stability analysis predicts two critical speeds at 6,000 (conical mode) and 18,000 rpm (first bending mode) respectively. Both modes are predicted to be stable for all speed and L/D ratios. Synchronous response at the mid-span for Case A shows the peak response at the first critical speed is slightly reduced as L/D increases while the response at the second critical speed is increased for most of the cases. In addition, the second critical speed is reduced from 18,000 to 13,000 rpm, which is not a concern because it remains above the running speed. This was also the trend for convergent-tapered hole-pattern seal. In addition, the increase of radial clearance in Case B slightly increases the amplitude of vibration, compared to Case A.

ACKNOWLEDGEMENTS

I would like to especially thank Dr. Dara Childs for granting me the opportunity to work with him and for providing essential guidance throughout my research project.

I cannot end without thanking my brother, Francisco Rodrigues, my father, Manuel Rodrigues, and my husband, Daniel van der Velde, on whom constant encouragement and love I have relied throughout my time at Texas A&M University. I am grateful also for the example of my mother, Celia Rodrigues. Her persistent courage and conviction will always inspire me, and I hope to continue, in my own small way, the noble mission to which she gave her life. It is to them that I dedicate this work.

TABLE OF CONTENTS

Page

Page

LIST OF FIGURES

FIGURE Page

FIGURE Page

FIGURE Page

FIGURE Page

LIST OF TABLES

NOMENCLATURE

C_r	Radial Clearance	[L]
C	Direct Damping	[FT/L]
c	Cross-coupled Damping	[FT/L]
C_{eff}	Effective Damping	[FT/L]
D	Seal Diameter	[L]
E	Modulus of Elasticity	[F/L^2]
f	Reaction Force Vector	[F]
K	Direct Stiffness	[F/L]
k	Cross-coupled Stiffness	[F/L]
K_{eff}	Effective Stiffness	[F/L]
L	Seal Length	[L]
N	Rpm	[1/T]
P	Pressure	[F/L^2]
R	Gas Constant	[FL/(MT)]
T	Temperature	[Θ]
X,Y	Displacement Directions	[L]
$\dot{X},\dot{Y}$	Velocities	[L/T]
$\dot{m}$	Mass Flow Rate	[M/T]
γ	Gamma Factor	[-]
μ	Absolute Viscosity	[F.T/L^2]
ρ	Density of Gas	[M/L^3]
Ω	Excitation Frequency	[1/T]
ω	Running Speed	[1/T]
$\omega_{critical}$	Critical Speed	[1/T]

Contractions

BTB	Back-to-back	[-]
C.G.	Center of Gravity	[L]
pk-pk	Peak to Peak	[-]

PR	Pressure Ratio	[-]
PS	Preswirl Ratio	[-]

Subscripts

in	Inlet	[-]
ex	Exit	[-]
R	Seal Reservoir value	[-]
S	Seal Sump value	[-]

INTRODUCTION

Injection compressors require comparatively long annular seals with high pressure drops across them that have a significant impact on rotordynamic characteristics. High pressure compressors are designed with stages arranged in either the in–line or back-to back configuration of Figure 1.

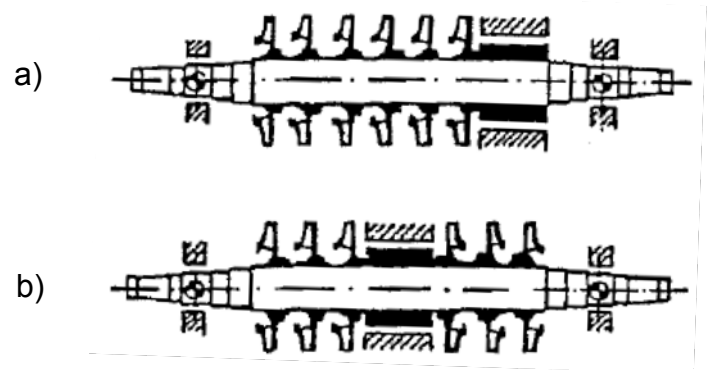

Figure 1 a) In-Line and b) Back-to-back Compressor Configurations [1]

In the in-line or straight-through compressor, the flow goes from stage to stage in a straight line, entering from the left and discharging on the right. For the back-to-back configuration, flow enters from the left to right through the first three stages, and then follows a cross-over duct to the right-hand side of the machine, and continues from right to left through the last three stages, discharging at the center. A major advantage of this design is that smaller axial thrust is produced in contrast to in-line configurations [1]. Figure 2 shows the locations of annular seals within a typical centrifugal compressor.

This thesis follows the style and format of the ASME Journal of Engineering for Gas Turbines and Power.

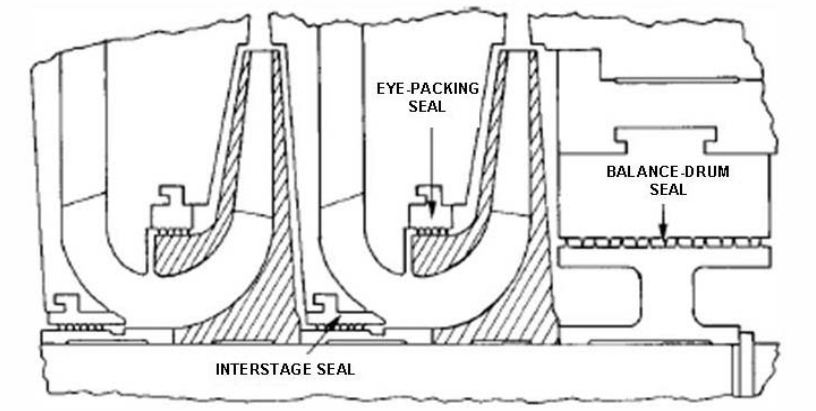

Figure 2 Annular Seal Locations for a Typical In-line Centrifugal Compressor [1]

For a straight-through compressor, the balance piston seal absorbs the full head rise of the machine, and it is used to limit axial thrust. In this configuration, the pressure ratio across the balance piston seal is typically between 40 and 50%. For a back-to-back compressor, the division wall seal is roughly centered at rotor mid-span and absorbs about one half of the machine's head rise, and deals with higher density gas. In addition, back-to-back compressors have pressures ratios across the division-wall seal of 50 to 60%.

LITERATURE REVIEW

Most of the initial rotordynamic instabilities experienced with centrifugal compressors were resolved by increasing the first critical speed through stiffening the rotor and/or shortening the bearing span. Fowlie and Miles [2] presented the case of three large centrifugal compressors (the Kaybob compressors) with severe instability problems which were resolved only by increasing the first critical speed through shortening the rotor and increasing the shaft diameter. Also, Fulton [3] cited another case where the increase of the first critical speed through reducing the bearing span and reducing the balance piston diameter had a decisive influence on the instability of a centrifugal compressor.

For rotor stability evaluation of high pressure machines, Fulton [3] proposed a "Rotor Stability Criteria" based on the "flexibility ratio" and the average gas density. Sood [4] defined the rotor flexibility ratio as the ratio of maximum continuous speed and the first critical speed on stiff support. Figure 3 illustrates the rotor stability plot.

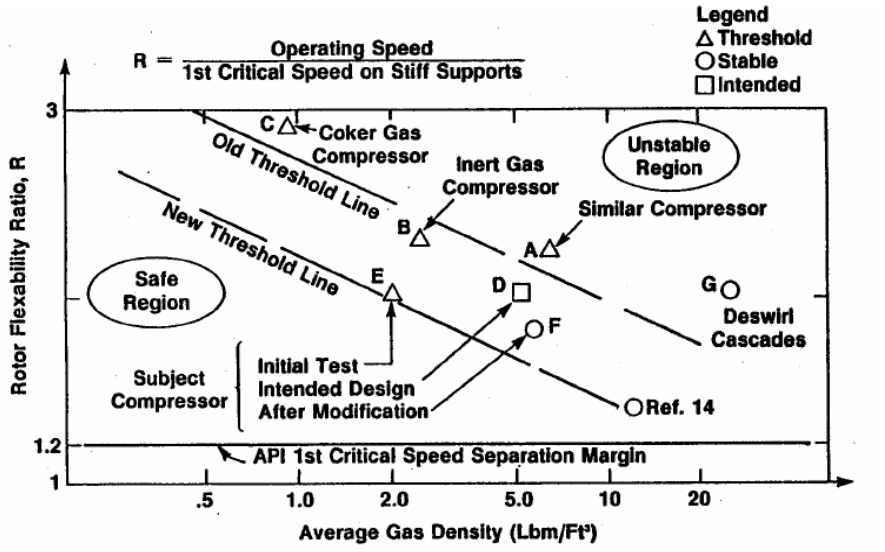

Figure 3 Rotor Stability Plot. Fulton [3]

The lines represent the approximate threshold condition where subsynchronous vibration could occur. Note that going above the line implies an increasing tendency for subsynchronous vibration to occur while staying below the line indicates that the rotor is less susceptible to such vibration. Increasing gas density slopes down the line, because high gas forces acting on the rotor require the increase of rotor stiffness to resist subsynchronous vibration. Hence, stiffening the rotor to increase the first critical speed implies a low flexibility ratio, and thus a more likely stable rotor.

Since the 1960s, annular seals using smooth rotors and honeycomb stators have been used in some petrochemical compressors, providing significant impact on stability and rotor response. Figure 4 shows a hole-pattern-stator seal.

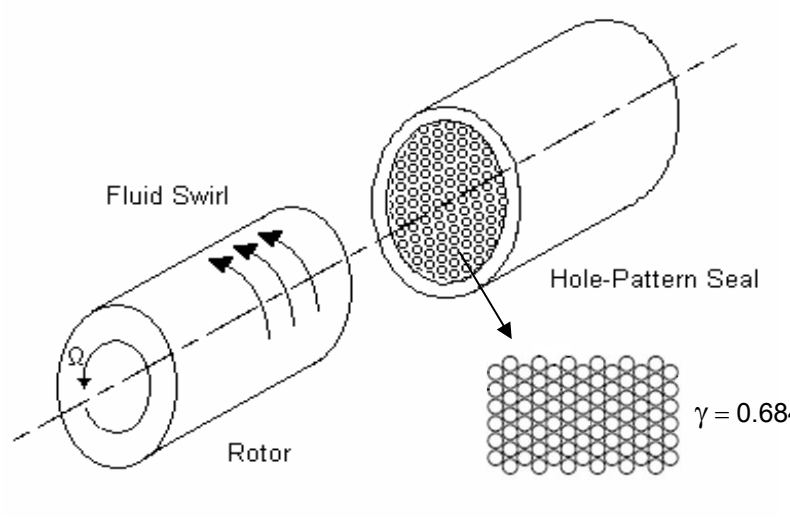

Figure 4 Hole-Pattern Seal [9]

Hole-pattern seals are basically a plain-seal that has had many radial holes drilled partially through it from the inside outward. The hole-pattern on the surface of the seal can be manufactured using a milling (round hole) or electrical discharge machining (honeycomb pattern). In Figure 4, gamma factor, γ, represents the hole-area density factor that is the fraction of area taken by the holes. Hole-pattern seals are generally manufactured more quickly and less expensively than honeycomb seals, and use softer materials; therefore, reducing the possibility of damage during rubs.

For motion about a centered position, Kleynhans and Childs [5] developed the following model for honeycomb and hole-pattern gas seals,

$$-\begin{Bmatrix} f_{sX} \\ f_{sY} \end{Bmatrix} = \begin{bmatrix} K(\Omega) & k(\Omega) \\ -k(\Omega) & K(\Omega) \end{bmatrix} \begin{Bmatrix} X \\ Y \end{Bmatrix} + \begin{bmatrix} C(\Omega) & c(\Omega) \\ -c(\Omega) & C(\Omega) \end{bmatrix} \begin{Bmatrix} \dot{X} \\ \dot{Y} \end{Bmatrix} \tag{1}$$

where K, k, C, and c are the frequency-dependent direct stiffness, cross-coupled stiffness, direct damping and cross-coupled damping, respectively. In addition, $\boldsymbol{f}_s$ is the reaction force vector; X and Y are the relative displacements between the sea and the rotor. Effective stiffness K_{eff} and effective damping C_{eff} are also function of the excitation frequency as defined in Equations (2) and (3).

$$K_{eff} = K(\Omega) + \Omega c(\Omega) \tag{2}$$

$$C_{eff} = C(\Omega) - \frac{k(\Omega)}{\Omega} \tag{3}$$

C_{eff} combines C, the stabilizing direct damping coefficient, and k, the destabilizing cross-coupled stiffness coefficient. Definitions apply only for small motion about a centered position.

Kleynhans and Childs' model predicted that hole-pattern seals have a strongly frequency dependent stiffness and damping coefficients. For high pressure centrifugal compressors, the predicted direct stiffness values at the running speed can be on the same order or higher than the bearings, and this implies that back-to-back machines could possibly accept more stages without instability problems.

Several test results for honeycomb and hole-pattern seals have validated Kleynhans and Childs predictions. Dawson [6] presents results for a honeycomb-stator/smooth-rotor seals and showed that its rotordynamic characteristic are frequency-dependent. In addition, Holt [7] tested two hole-pattern-stator seal with different cell depths, and he measured strongly frequency dependent direct stiffness and damping values, supporting Kleynhans and Childs model and predictions. In addition, he

showed that an increase in hole depth increased the effective stiffness while decreasing the effective damping.

Subsequent tests to support the predictions were performed by Weatherwax and Childs [8] at a supply pressure of 70 bars and different eccentricities to examine the effect of eccentricity on the rotordynamic characteristics and leakage. Their results showed good agreement with predictions with no effect on rotordynamic and leakage characteristics up to 50% eccentricity ratio.

Wade [9, 10] tested a hole-pattern gas seal to determine the influence of testing parameters such as pressure ratio, inlet fluid preswirl, rotor speed, and radial clearance. He also tested the seal under choked flow conditions, and found that there was not a significant change in seal behavior when the seal transitioned to the choked condition. His results showed that the pressure ratio, inlet fluid preswirl, speed, and specially the radial clearance caused a significant effect on the rotordynamic characteristics of the seals, in good agreement with theory predictions.

Sprowl [11] compared constant clearance smooth and honeycomb annular gas seals. His measurement confirmed the frequency-dependent nature of the honeycomb seal for all level of preswirl in good agreement with prediction, especially at 35% and 50% backpressure. However, for low backpressures, there are some discrepancies between measurements and theory for K values that may be due to the theoretical prediction of choked flow in the seal. In summary, all these results have confirmed the prediction accuracy of Kleynhans and Childs' two-volume model.

Honeycomb and hole-pattern seals have been used to eliminate or reduce rotordynamic stabilities in several industrial turbomachines by developing large stiffness and damping coefficients. For instance, Childs and Moyer [12] discuss an application of honeycomb seals to eliminate rotordynamic instabilities of the High Pressure Oxygen Turbopump of the Space Shuttle Main Engine. Zeidan et al. [13] eliminated chronic instabilities in two centrifugal gas compressors by replacing labyrinth seals with honeycomb seals. Also, Sorokes, et al. [14] eliminated a stability problem for a high pressure compressor replacing a labyrinth with a honeycomb seal. Armstrong and Perricone [15] used the same approach to eliminate rotordynamic instability in a steam turbine. Recently, Moore et al. [16] presented test results for a back-to-back centrifugal

compressor that used a hole-pattern division-wall seal to remarkably good effect, improving the compressor's stability with increasing differential pressure.

OBJECTIVES

One of the significant subjects that will be investigated through this analysis is the influence of implementing much longer hole-pattern seals on back-to-back compressors with seal at mid-span and in-line compressors with the seal at 82% of rotor span, in regard to their impact on rotordynamic stability, synchronous response, and leakage.

Another important point that will be addressed is the predicted impact of convergent-tapered hole-pattern seal, and seal clearances as design parameters.

Finally, the compressors dynamic characteristics for mechanical test condition (in the absence of pressure) will be investigated for each increased rotor length, and the improvement on the response of the rotor at this condition will be shown.

To achieve these objectives, this study compares predicted rotordynamic coefficients of different seal configurations for different L/D ratios. Also, stability analysis and synchronous response for different L/D ratios will be compared to understand the influence of these parameters on the performance of representative compressors.

DESCRIPTION OF THE ROTORDYNAMIC MODEL

Figure 5 shows the rotordynamic model of a seven-stage, back-to-back (BTB) natural gas centrifugal compressor with a nominal speed of 10,000 rpm. For simplicity, the model does not include lumped masses for the compressor wheels. The total bearing span of the compressor rotor is 1.27 m, with a total mass of 142.66 kg. This model includes bearing support mass equivalent to 22.73 kg, and a coupling mass of 6.35 kg attached on the left end of the rotor. Its center of gravity (C.G.) is approximately 0.608 m from the left end of the rotor. Five-pad tilting pad bearings (with load between pads configuration) support the rotor at both free ends. Left and right bearings are placed at 6.35 cm from both ends.

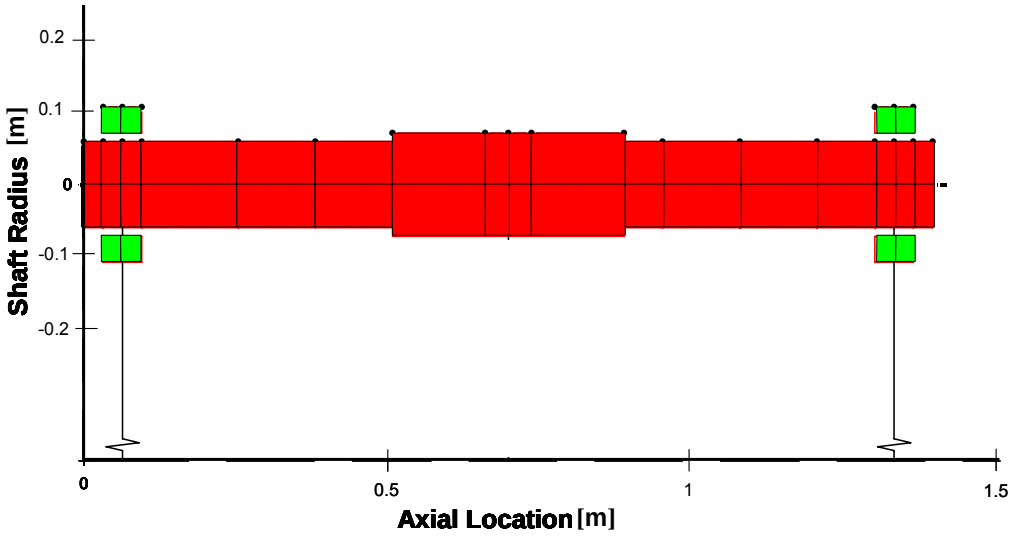

Figure 5 Rotordynamic Model of Natural Gas Centrifugal Compressor

The synchronous response plots at bearing location and bearing mid-span are shown in Figures 6 and 7, with 144.02 gr-mm of unbalance at the bearing mid-span. The model contained only the bearing reaction forces (no seals). The predicted first and second critical speeds are 5,000 and 18,000 rpm, respectively. Note that the response plots show a well-damped first critical speed. At bearing mid-span, the critical-speed responses are larger than that at bearing location.

The first critical speed is associated with a cylindrical mode, and the second critical speed is associated with the bending mode. Both modes are predicted to be always stable (log dec > 0). Figures 8 and 9 illustrate the first and second mode shape of the system.

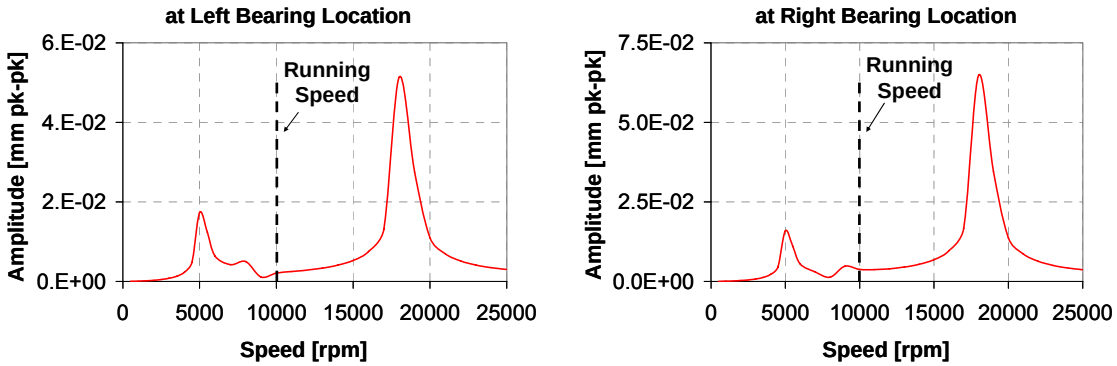

Figure 6 Synchronous Response to Unbalance at Both Bearing Locations for the Rotor Model supported by Tilting Pad Bearings

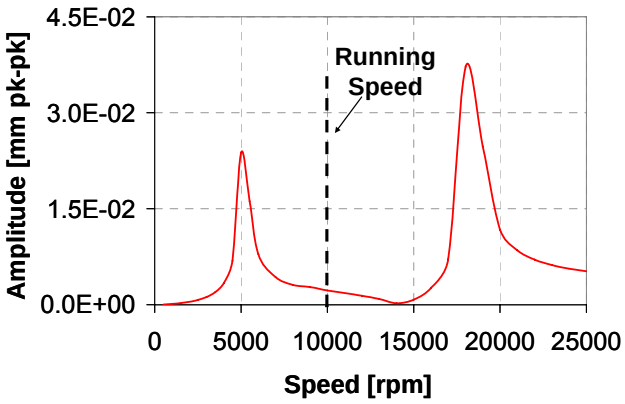

Figure 7 Synchronous Response to Unbalance at Mid-span for the Rotor Model supported by Tilting Pad Bearings

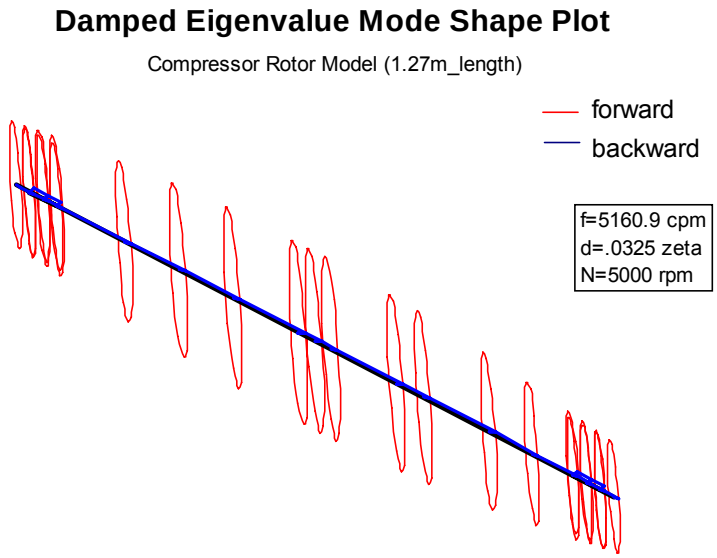

Figure 8 Rotor Mode Shape at the First Critical Speed with Tilting Pad Bearings

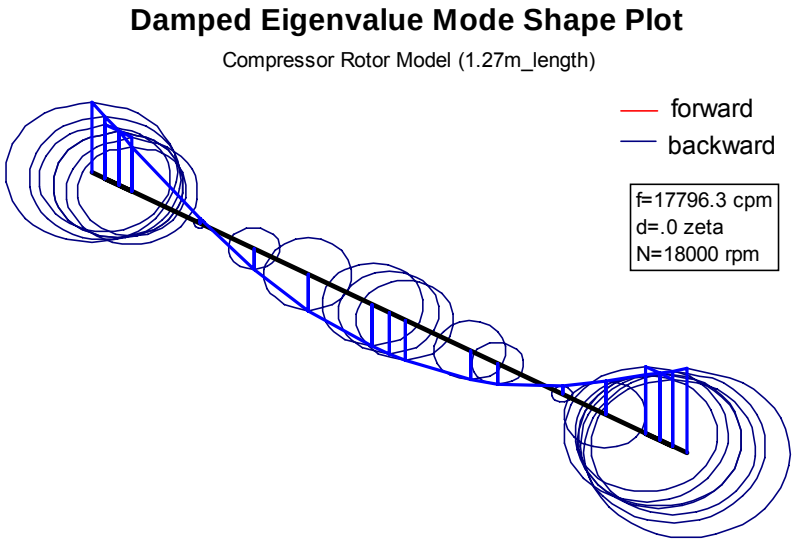

Figure 9 Rotor Mode Shape at the Second Critical Speed with Tilting Pad Bearings

DESCRIPTION OF PROCEDURE AND CONFIGURATIONS

Leakage and rotordynamic coefficients will be calculated for hole-pattern seals that have L/D ratios of 0.5, 1, 1.5, 2, and 2.5. Lengthening the hole-pattern seals implies a better rotordynamic performance because the seal's stiffness and damping coefficients increases, while the leakage decreases. However, the increase in seal length implies an increment in the bearing span, and it lowers the first critical speed of the system.

Equation (4) shows that the first natural frequency for a uniform cylindrical beam with pinned ends is,

$$\omega_{natural} = \sqrt{\frac{3E}{\rho}} \cdot DL^{-2} \tag{4}$$

showing that the natural frequency is inversely proportional to the bearing span squared. This dependency and the Fulton diagram of Figure 3 have caused a strong resistance to increasing bearing span of compressors.

The hole-pattern seal leakage and rotordynamic coefficients will be predicted using a code (based on a constant temperature bulk-flow model) developed by Kleynhans and Childs [4]. It is important to remark that this code does not include moment coefficients; parameters than can effect the results. All the coefficients will be calculated at a pressure ratio of 0.5. The pressure ratio is defined as the exit pressure divided by the inlet pressure. Table 1 shows the input parameters required.

Table 1 Seal Dimensions and Input Parameters

Seal Diameter	0.1524 [m]
L/D Ratio	0.5, 1, 1.5, 2, 2.5
Inlet Clearance	0.3048 [mm]
Exit Clearance	0.3048 [mm]
Cell Volume / Area Ratio	3.299 [mm]
Reservoir Pressure P_R	34.474 10^6 [Pa]
Sump Pressure P_S	17.237 10^6 [Pa]
Reservoir Temperature T_R	104.44 [ºC]
Operating Speed ω	10000 [rpm]
Gamma Factor γ	0.684
Inlet Preswirl Ratio	0
Absolute Viscosity μ	2.0 10^{-5} [Pa sec]
Molecular weight	16.043
Specific heat ratio	1.299

All the predicted stiffness and damping coefficients for hole-pattern seals are strongly frequency dependent; therefore, these “synchronous” rotordynamic coefficients, to be used in the synchronous response, were calculated using the values at the running speed for each respective case. Figures 10 and 11 illustrate the plots of the frequency dependent $K(\Omega)$, $k(\Omega)$, $C(\Omega)$, and $c(\Omega)$ for constant clearance and convergent-tapered hole-pattern seals with L/D ratio of 0.5.

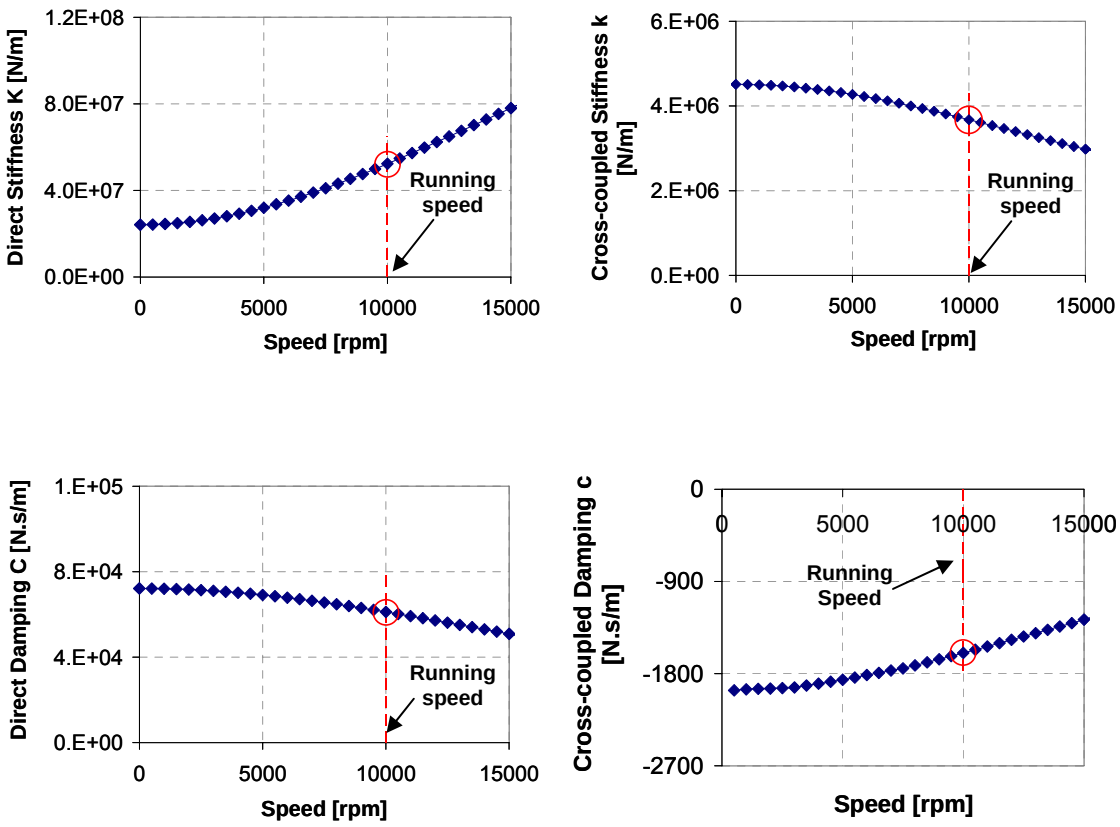

Figure 10 Direct and Cross-coupled Stiffness and Damping Coefficients for Constant Clearance Hole-Pattern Seal with L/D Ratio of 0.5

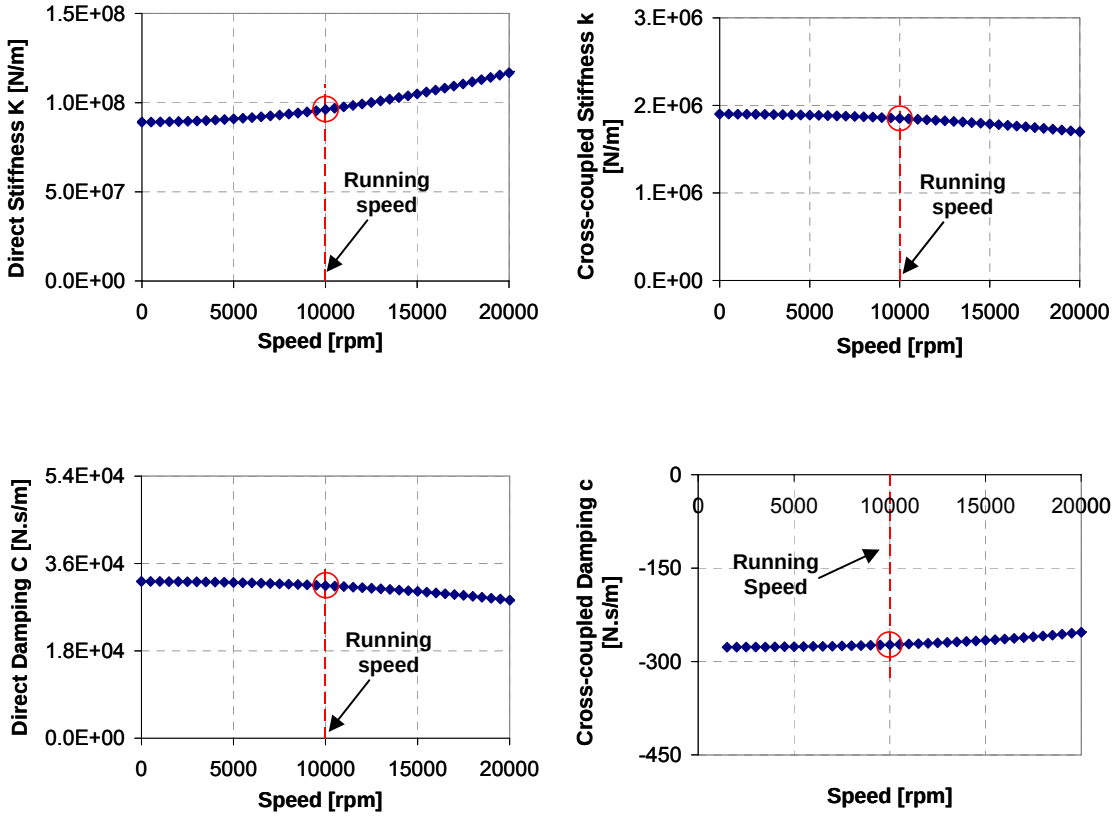

Figure 11 Direct and Cross-coupled Stiffness and Damping Coefficients for Convergent-Tapered Hole-Pattern Seal ($C_{rin}/C_{rex} = 2$) with L/D Ratio of 0.5

Note from the plots that the direct stiffness for convergent-tapered hole-pattern seal is greater than for constant clearance hole-pattern seal. With constant clearance seals, low or even negative direct stiffness values can occur especially at low frequencies. The use of convergent-tapered hole-pattern seal completely eliminates this undesirable situation, a reason that supports the use of convergent-tapered seals.

Due to the pressure and frequency dependency of the hole-pattern seal, seal coefficients will be calculated at 500 rpm increments from 500 rpm to 15000 rpm, with its corresponding pressure supply value. Figure 12 shows the linear pressure versus speed relationship used to calculate the rotordynamic coefficients of the hole-pattern seal.

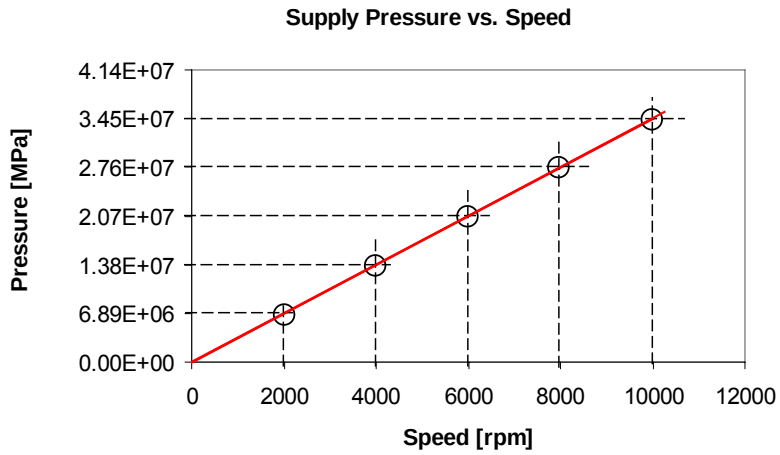

Figure 12 Pressure-running Speed Dependent Relationship Plot

Separate rotor models will be developed for each increased seal length. The seal's effect on each compressor rotor model will be presented at two alternative locations: for a back-to-back compressor with seal at mid-span, and a in-line compressor with seal at 82% of the rotor span.

This analysis will include the influence on injection compressors of both constant clearance and convergent-tapered hole-pattern seals, as well as the influence of clearance as a design parameter. Table 2 shows the cases to be considered in this analysis. For case B, calculations were performed to select an increased clearance that would maintain the same leakage as the original with L/D=0.5. Those larger radial clearances were chosen to minimize rubbing at seal location.

Table 2 Cases Performed for Each Rotordynamic Model

	L/D	Inlet Clearance [mm]	Exit Clearance [mm]	Description
CASE A	0.5	0.3048	0.3048	Constant-clearance constant clearance hole-pattern seal as L/D increases
	1	0.3048	0.3048	
	1.5	0.3048	0.3048	
	2	0.3048	0.3048	
	2.5	0.3048	0.3048	
CASE B	0.5	0.3048	0.3048	Increasing C_r, to have the same leakage as Case A for L/D = 0.5
	1	0.3683	0.3683	
	1.5	0.4191	0.4191	
	2	0.4547	0.4547	
	2.5	0.4851	0.4851	
CASE C	0.5	0.6096	0.3048	Convergent-tapered hole-pattern seal with $C_{rin} / C_{rex} = 2$ as L/D increases
	1	0.6096	0.3048	
	1.5	0.6096	0.3048	
	2	0.6096	0.3048	
	2.5	0.6096	0.3048	

COMPARISON OF ROTORDYNAMIC CHARACTERISTICS FOR LONGER HOLE-PATTERN SEALS

This section illustrates and compares the synchronous rotordynamic characteristics and leakage of constant clearance and convergent-tapered hole-pattern seals with L/D ratios of 0.5, 1, 1.5, 2, and 2.5. In addition, the results presented show the influence of radial seal clearance as a design parameter. A code based on the work of Kleynhans and Childs is used to predict all the coefficients. Table 1 shows the input parameters required. Note that the moment coefficients are not included in this code.

All the predicted stiffness and damping coefficients for hole-pattern seals were calculated using the results from Figures 10-12 to establish the seal coefficients at each speed to be used in the synchronous response.

The zero preswirl condition and the 50% pressure ratio are used in all calculations. Parameters of interest reported are direct and cross-coupled stiffness and damping, effective stiffness and damping, leakage flow rate and static stiffness, for each case describe in Table 2.

Synchronous Direct and Cross-coupled Stiffness

The effect of lengthening the seals on direct and cross-coupled stiffness for all cases is presented in Figures 13 through 15. One interesting trend observed in each case is the increase of direct stiffness as L/D increases. In general, L/D of 2.5 shows the greatest overall direct stiffness as speed increases for all cases. Note from Figure 12 that for L/D > 1.5, the direct stiffness is reduced.

Looking at the plots of direct stiffness across the three cases presented, the hole-pattern seals exhibit an increase in direct stiffness as rotational speed increases for Each L/D, showing speed-dependent direct stiffness. These plots show that the direct stiffness for the convergent-tapered hole-pattern seal is smaller than the constant clearance hole-pattern seal for L/D > 0.5. These results do not agree with Fleming's predictions [17] that a convergent-tapered-bore seal has significantly more direct stiffness than constant clearance seals. The increase in radial clearance for constant

clearance hole-pattern seals as L/D increases causes a decrease of direct stiffness compared to case A.

An increase of cross-coupled stiffness is visible as L/D increase for all cases. In addition, cross-coupled stiffness increases as rotational speed increases. The convergent-tapered hole-pattern seal exhibits larger cross-coupled stiffness than the constant clearance hole-pattern seal for all L/D. In addition, the increase in radial clearance as L/D increases for constant clearance seal slightly decreases the cross-coupled stiffness.

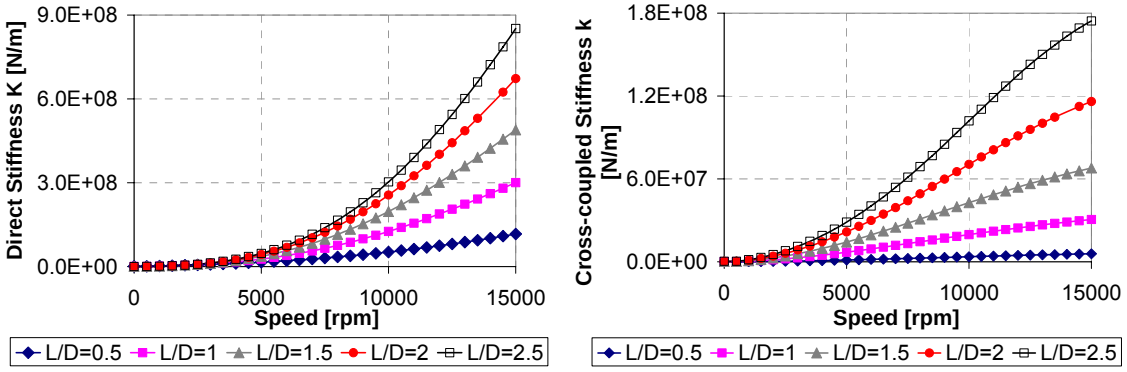

Figure 13 Synchronous Direct and Cross-coupled Stiffness versus Shaft Speed with 50% Pressure Ratio for Constant Clearance Hole-Pattern Seals as L/D Increases (Case A)

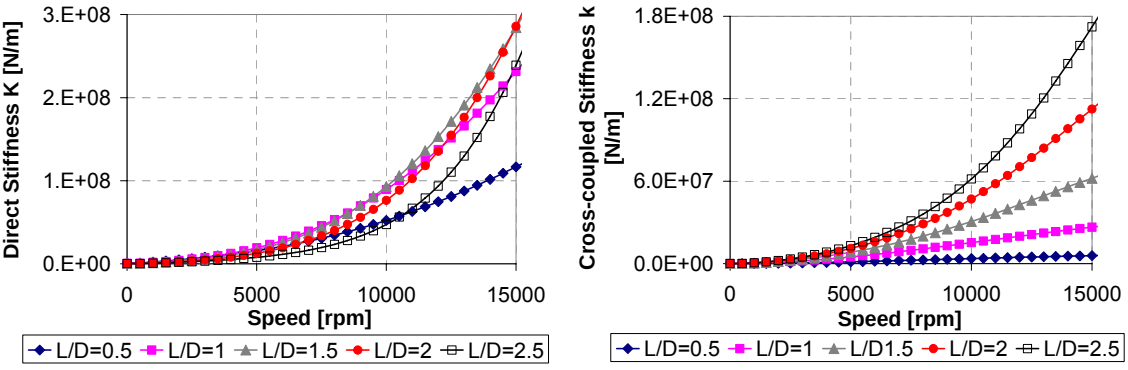

Figure 14 Synchronous Direct and Cross-coupled Stiffness versus Shaft Speed with 50% Pressure Ratio Increasing Radial Seal Clearance, Holding Leakage Constant as L/D Increases (Case B)

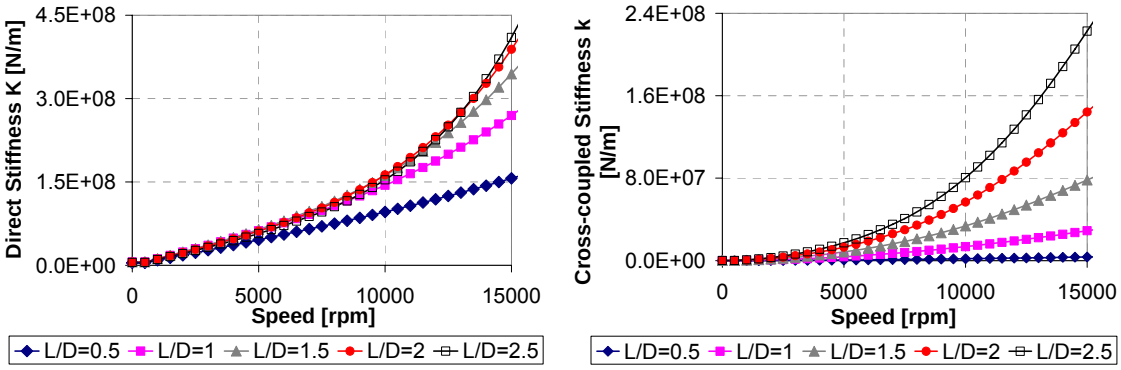

Figure 15 Synchronous Direct and Cross-coupled Stiffness versus Shaft Speed with 50% Pressure Ratio for Convergent-Tapered Hole-Pattern Seal with $C_{r\,in} / C_{r\,ex} = 2$ as L/D Increases (Case C)

Synchronous Direct Damping

Comparisons of direct damping for increased seal length of constant clearance and convergent-tapered hole-pattern seals are illustrated in Figures 16 through 18.

For all cases, an increase of the direct damping is visible across the speed range as L/D increases, since the direct damping is roughly proportional to the differential pressure, which is increasing linearly with speed. Note that the greater magnitude of direct damping occurs at L/D ratio of 2.5.

The constant clearance hole-pattern seal exhibit on average larger direct damping for each L/D ratio than that for the convergent hole-pattern seals.

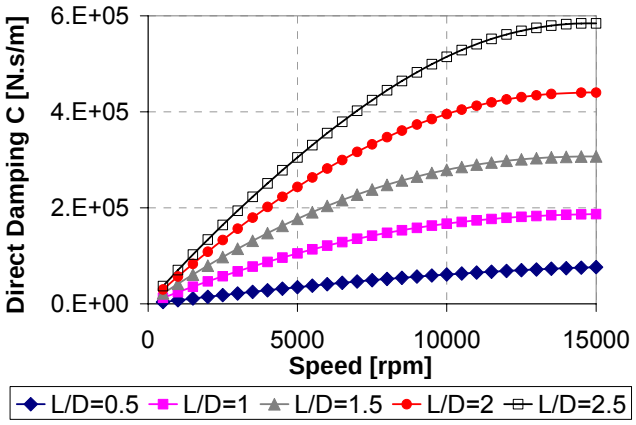

Figure 16 Synchronous Direct Damping versus Shaft Speed with 50% Pressure Ratio for Constant Seal Clearance as L/D Increases (Case A)

Figure 17 illustrates the effect of increasing clearances to keep leakage constant for a constant clearance hole-pattern seal while increasing L/D. Note that the direct damping is smaller because of the increase in clearance for each L/D ratio, compared to case A.

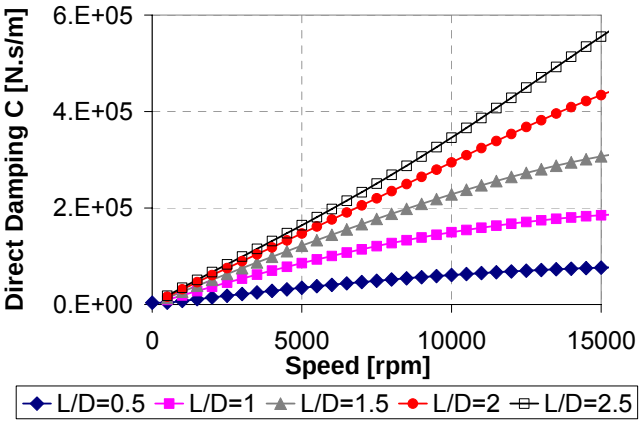

Figure 17 Synchronous Direct Damping versus Shaft Speed with 50% Pressure Ratio Increasing Radial Seal Clearance, Holding Leakage Constant as L/D Increases (Case B)

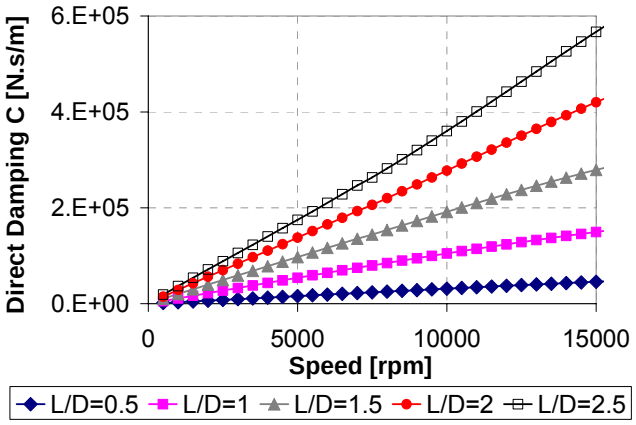

Figure 18 Synchronous Direct Damping versus Shaft Speed with 50% Pressure Ratio for Convergent-Tapered Hole-Pattern Seal with $C_{r\,in} / C_{r\,ex} = 2$ as L/D Increases (Case C)

From Figure 18, an increase of direct damping as L/D increases is visible for case C. The direct damping for convergent-tapered seal shows a stronger linear relationship as speed increases, compared to that with constant clearance seals, especially at speed higher than 10,000 rpm.

Synchronous Effective Stiffness and Damping

Effective stiffness (K_{eff}) and damping (C_{eff}) were defined previously in Equations (2) and (3). Comparisons of effective stiffness and damping for different seal length are presented in Figures 19-21.

In general, the effective stiffness increases as seal length increases, showing large effective stiffness values at high speeds. The largest effective stiffness value is on the order of magnitude of approximately 10^8 N/m.

Looking at the effective stiffness plots for constant clearance and convergent-tapered hole-pattern seals, the constant clearance seals exhibit larger effective stiffness than the convergent-tapered hole-pattern seals at all L/D ratios. In addition, the effective stiffness of constant clearance at each L/D ratio is decreased when their radial clearance is increased, keeping leakage constant.

The effective damping of the seal is one of the best indicators in determining the stability of a roughened stator annular gas seal. For all seals, the effective damping visibly increases as L/D increases. The constant clearance seal exhibits on average larger effective damping than the convergent-tapered hole-pattern seal at any L/D ratio, especially at lower speeds.

In addition, the effective damping value is reduced with increasing radial clearance for all L/D ratios.

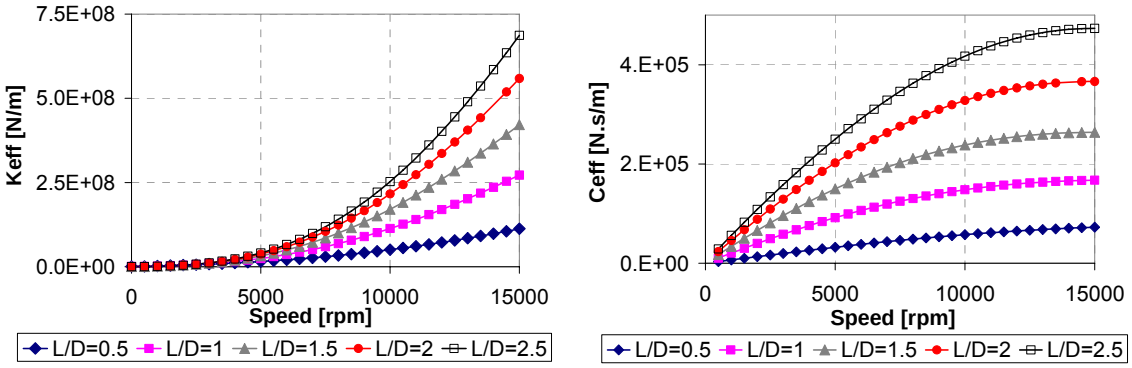

Figure 19 Synchronous Effective Stiffness (K_{eff}) and Damping (C_{eff}) versus Shaft Speed with 50% Pressure Ratio for Constant Seal Clearance as L/D Increases (Case A)

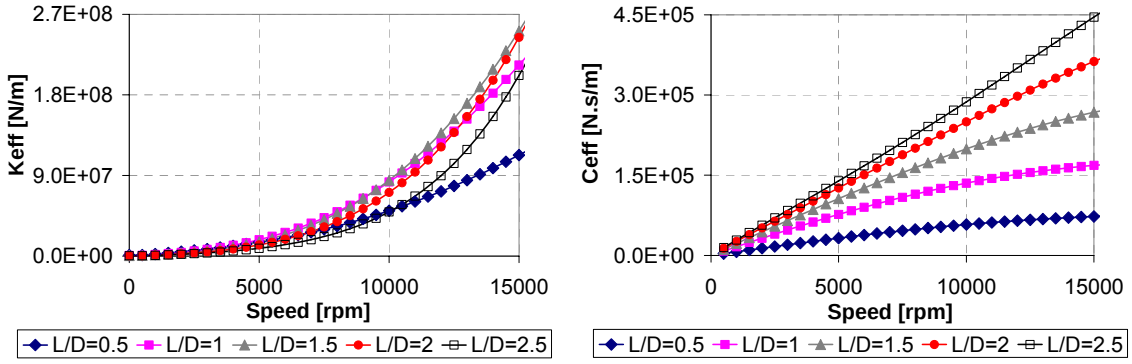

Figure 20 Synchronous Effective Stiffness (K_{eff}) and Damping (C_{eff}) versus Shaft Speed with 50% Pressure Ratio Increasing Radial Seal Clearance, Holding Leakage Constant as L/D Increases (Case B)

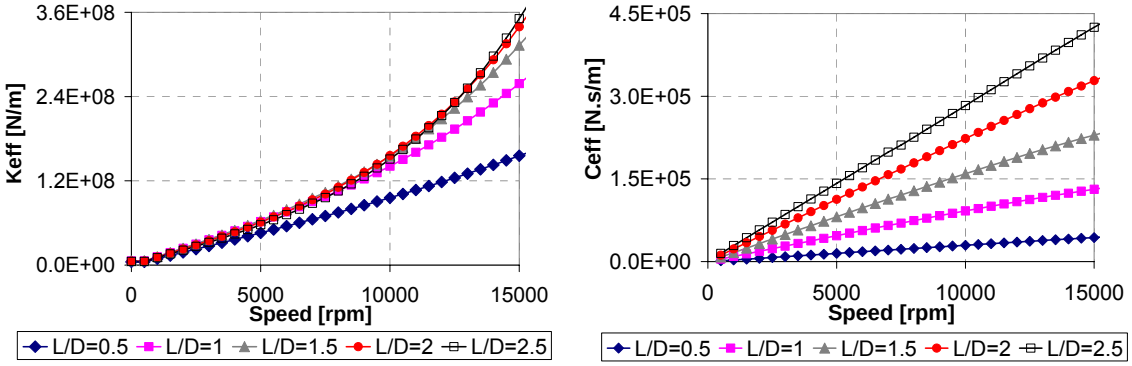

Figure 21 Synchronous Effective Stiffness (K_{eff}) and Damping (C_{eff}) versus Shaft Speed with 50% Pressure Ratio for Convergent-Tapered Hole-Pattern Seal with as L/D Increases (Case C)

Leakage Flow Rate

The effect of lengthening the seals on leakage performance is illustrated in Figures 20 through 22. As mentioned before, the code based on the work of Kleynhans and Childs is used to predict leakage for all conditions. This code uses a Blasius friction factor model shown in Equation 5.

$$f_f = n\,\mathrm{Re}^m \tag{5}$$

The values used for the Blasius friction factor model were n_{rotor} = 0.0586, m_{rotor} = -0.2170, n_{stator} = 0.0785, and n_{rotor} = -0.1101.

For both constant clearance and convergent-tapered hole-pattern seals, the leakage flow rate significantly decreases as the seal length increases. At L/D = 2.5, the constant clearance and convergent-tapered hole-pattern seals leak an average of 47 percent less than at L/D=0.5.

As shown in Figures 22 and 23, a significant reduction of leakage flow rate is observed from convergent-tapered hole-pattern seals to constant clearance hole-pattern seals. The increase in average clearance introducing a convergent-tapered seal increases leakage. At any L/D ratio, the constant clearance hole-pattern seal leaks an average of 35% less than the convergent-tapered hole-pattern seal.

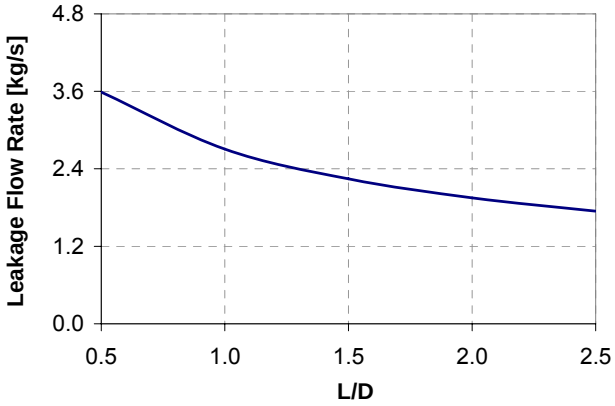

Figure 22 Leakage Flow Rate versus L/D for Constant Clearance Hole-Pattern Seal (Case A)

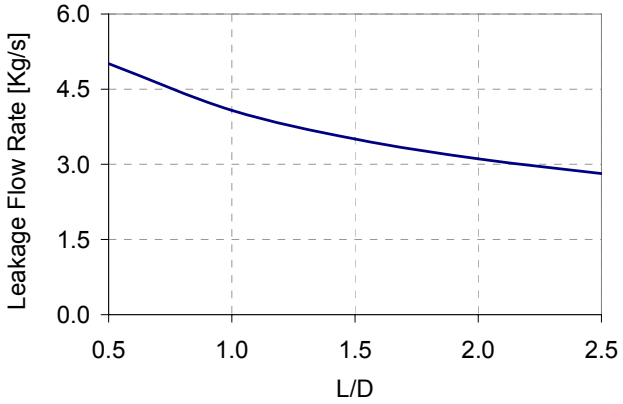

Figure 23 Leakage Flow Rate versus L/D for Convergent-Tapered Hole-Pattern Seal with $C_{r\,in} / C_{r\,ex} = 2$ as L/D Increases (Case C)

For case B, the increased radial clearance for each increased length was calculated to maintain the same leakage flow rate as the original one with L/D=0.5 (3.6 kg/s approximately).

Static Stiffness

The static stiffness, K_{static}, is the zero-frequency intercept for effective stiffness. Figures 24 through 26 show the static stiffness as L/D increases for all three cases.

From Figures 24 and 25, a significant reduction of the static stiffness as L/D increases is observed. For case A, a reduction of approximately 80 percent is observed as L/D increases from 0.5 to 2.5. For case B, the reduction of static stiffness is approximately 76 percent with increasing L/D from 0.5 to 2.5. In addition, for case B the static stiffness drops faster as L/D increases from 0.5 to 2 than for case A.

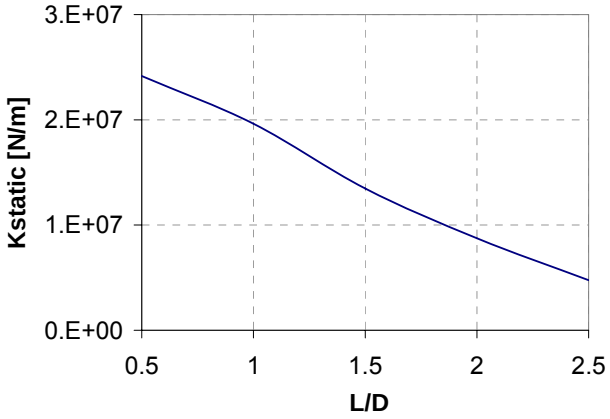

Figure 24 Static Stiffness versus L/D Ratios for Case A

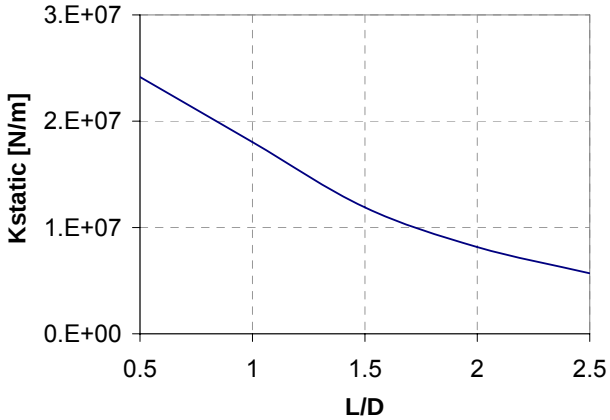

Figure 25 Static Stiffness versus L/D Ratios for Case B

Figure 26 shows the effect of convergent-tapered hole-pattern seals on the static stiffness as L/D increases. A reduction of 16 percent in static stiffness is observed with increasing L/D from 1 to 2.5. This tendency is not observed as L/D increases from 0.5 to 1.

Comparisons of the static stiffness for constant clearance and convergent-tapered seal indicate that convergent-tapered seals exhibit larger static stiffness values than constant clearance seals for all L/D ratios.

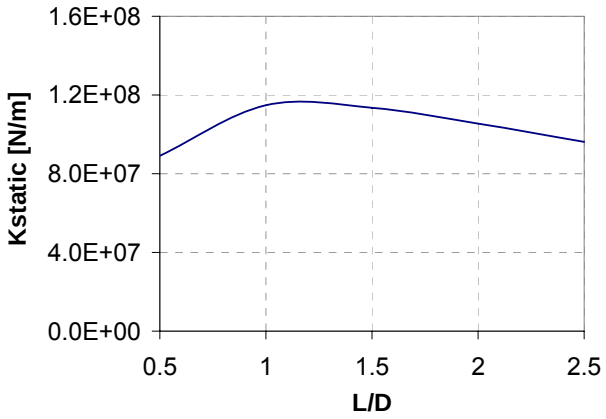

Figure 26 Static Stiffness versus L/D Ratios for Case C

PREDICTIONS OF STABILITY AND SYNCHRONOUS RESPONSE FOR REPRESENTATIVE COMPRESSOR WITH LONGER HOLE-PATTERN SEALS

This section presents and compares the stability analysis and the synchronous response for two representative compressors with longer seals. The effects of longer constant clearance and convergent-tapered hole-pattern seals on stability and linear response are presented at two alternative locations: for back-to-back compressor with seal at bearing mid-span, and for in-line compressor with seal at 82% of the bearing span.

The synchronous rotordynamic coefficients obtained for each hole-pattern seal configuration, are coupled to the rotordynamic model to perform a linear stability analysis. The stability model includes the tilting pad bearings, the bearing supports, and the hole-pattern seal. In addition, an estimated imbalance is used along with the rotordynamic coefficients of the model to calculate the synchronous response to unbalance for each L/D ratio.

Back-to-back Compressor with Seal at Mid-span

Stability Analysis

The key parameter used to analyze rotordynamic stability of the system is the logarithmic decrement or log dec. Figure 27 illustrate the stability map of the system for two different cases.

For all cases, the system logarithmic decrement was predicted to be positive over all speed range, which means that the system is stable. Note that for both cases, the log dec for the cylindrical modes remains almost constant with increasing running speed. However, the bending mode for the larger rotor becomes less stable as running speed increases, while for the shorter rotor becomes more stable with increasing running speed.

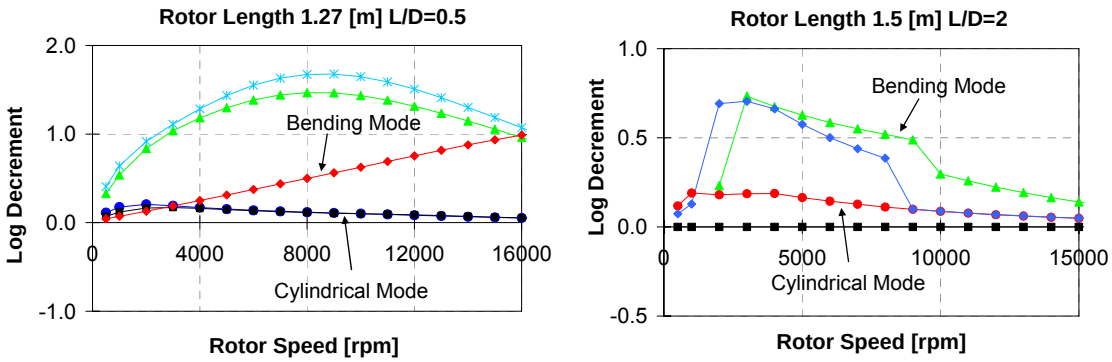

a) b)

Figure 27 Logarithmic Decrement versus Rotor Speed for a) Rotor Model of 1.27 m Length with Constant Clearance Hole-Pattern (Case A), and b) Rotor Model of 1.5 m Length with Convergent-Tapered Hole-Pattern Seal (Case B)

To compare the stability for the different cases, Figures 28 through 30 illustrate the damped natural frequencies versus damping exponent for all L/D ratios. The damping exponent determines whether the vibration will grows exponentially (unstable) or die out (stable). For all cases, the system is predicted to be stable (damping exponent < 0) for each L/D ratio. Note that for all the cases, the stability of the system is considerably improved as L/D increases.

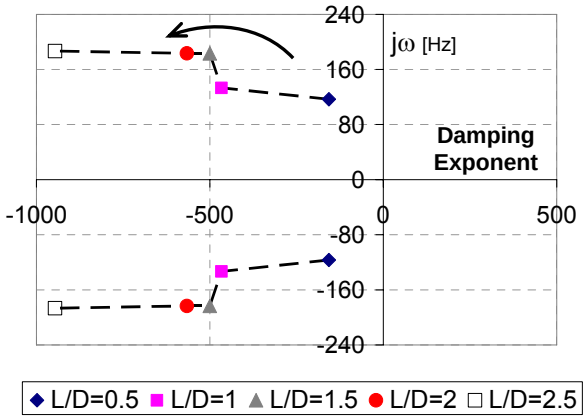

Figure 28 Damped Natural Frequency versus Damping Exponent for Case A with Seal at Mid-span for the First Critical Speed (8,000 rpm) Associated with a Cylindrical Mode

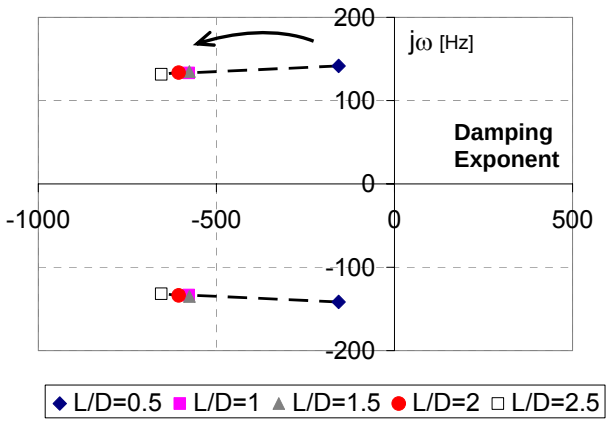

Figure 29 Damped Natural Frequency versus Damping Exponent for Case B with Seal at Mid-span for the First Critical Speed (8,000 rpm) Associated with a Cylindrical Mode

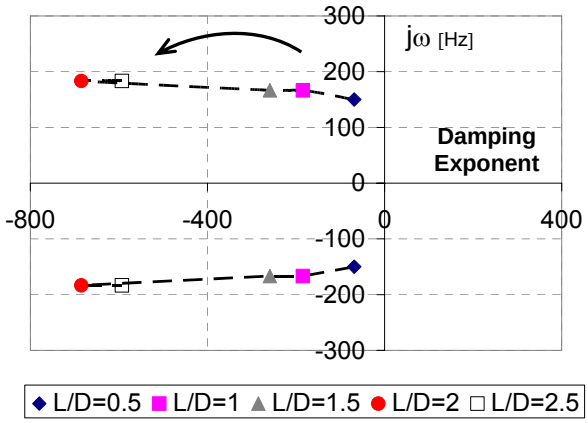

Figure 30 Damped Natural Frequency versus Damping Exponent for Case C with Seal at Mid-span for the First Critical Speed (9,000 rpm) Associated with a Cylindrical Mode

Synchronous Response to Unbalance

This section presents the influence on the synchronous response to unbalance of increasing L/D for a back-to back compressor with seal at mid-span for cases A, B, and C. The unbalance mass used for the synchronous response predictions is 144.02 gr-mm applied at the mid-span. This analysis is performed for different seal lengths, clearances, and for constant clearance and convergent-tapered hole-pattern seals.

Figures 31 and 32 illustrate the synchronous response at the bearings and mid-span for case A with seal at the mid-span at each L/D ratios.

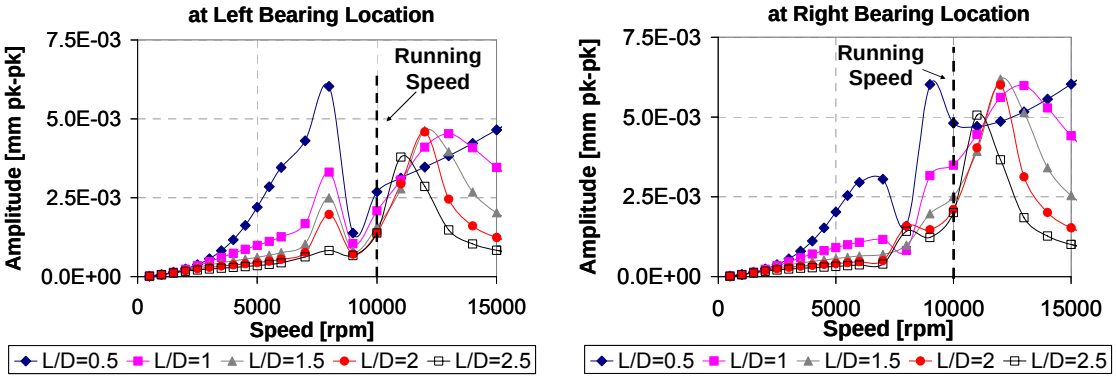

Figure 31 Synchronous Responses to Unbalance at Both Bearing Locations, Case A with Seal at Mid-span

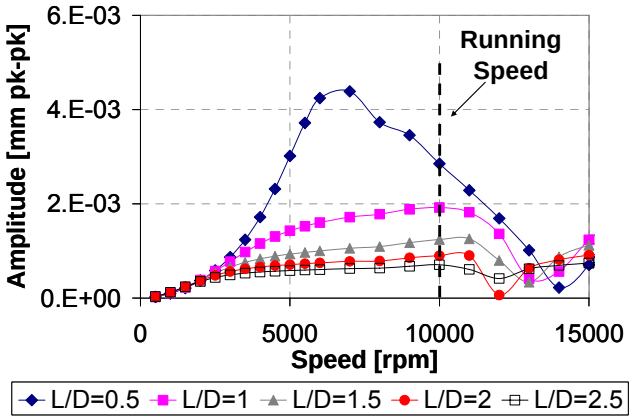

Figure 32 Synchronous Response to Unbalance at Mid-span, Case A with Seal at Mid-span

Note from Figure 31 that the first critical speed remains constant and the amplitude of vibration shows a significant reduction of approximately 86 percent as L/D is increased from 0.5 to 2.5, for both bearings. However, from 11,000 to 13,000 rpm approximately, the amplitude of vibration increases as L/D increases.

Looking at Figure 32, the synchronous response shows a critical speed at 8,000 rpm approximately. Comparison of the responses for each L/D reveals a significant reduction of approximately 85 percent in the response from $4.4*10^{-3}$ mm pk-pk to $6.3*10^{4}$ mm pk-pk. These results demonstrate a dramatic improvement of the synchronous response with increasing seal length.

Figure 33 illustrates the shaft deflections at the first critical speed of the rotor model for each L/D ratio, using a constant-clearance hole-pattern seal at bearing mid-span. The shaft deflection is reduced with increasing seal length.

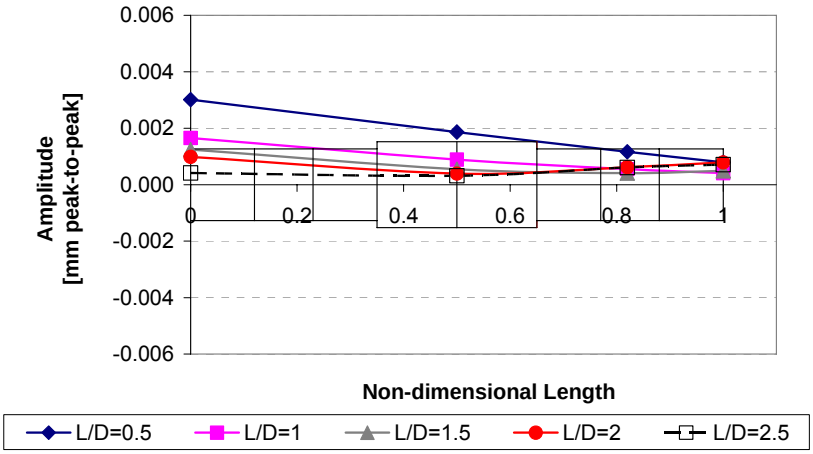

Figure 33 Shaft Deflection for Each L/D Ratio, Case A with Seal at Mid-span for the First Critical Speed (8,000 rpm)

Figures 34 and 35 compare the synchronous response at bearing locations and mid-span for all L/D ratios, for case B. The constant clearance hole-pattern seal is located at the bearing mid-span.

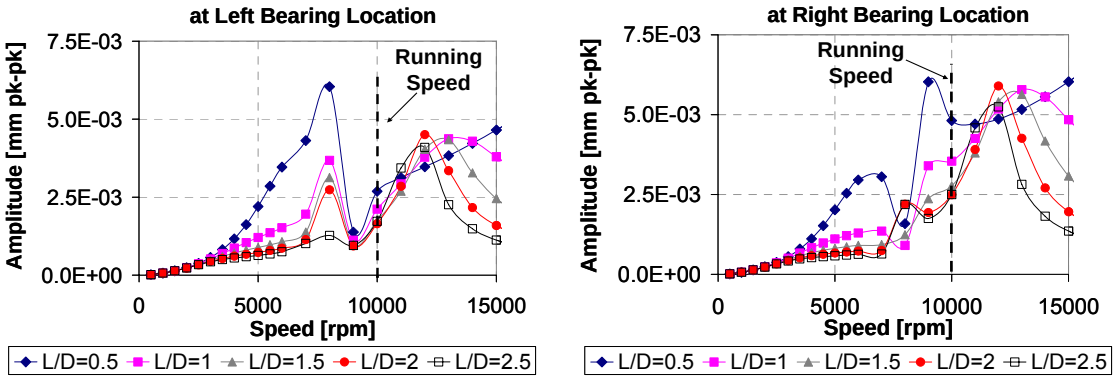

Figure 34 Synchronous Response to Unbalance at Both Bearing Locations, Case B with Seal at Mid-span

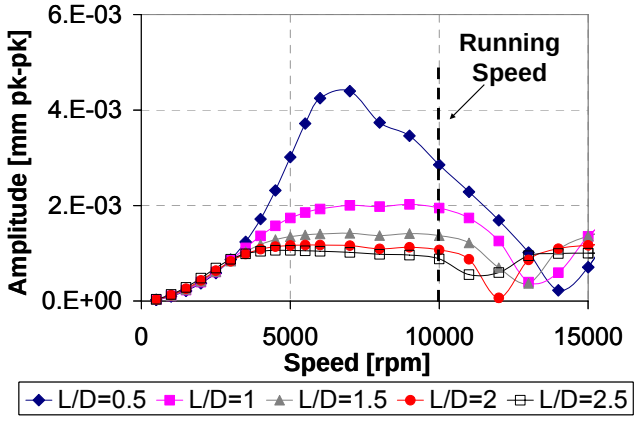

Figure 35 Synchronous Response to Unbalance at Mid-span, Case B with Seal at Mid-span

Note that at both bearing locations, the response of the first critical speed (8,000 rpm) is substantially reduced with increasing seal length. At both bearings, a reduction of approximately 79 percent in the response is observed with L/D increasing from 0.5 to 2.5. In addition, the response at the running speed is reduced as L/D increases, at both bearing locations.

Also a clearly reduction in response at the critical speed and running speed is exhibited at rotor mid-span. The model exhibits a reduction of approximately 77 percent in the response with L/D increasing from 0.5 to 2.5.

Comparison of case A and B reveals that the increment of radial seal clearance slightly affects the synchronous response of the system. Increasing the seal clearance as L/D increases slightly increases the amplitude of vibration compared to that with constant clearance, showing almost no effect on the response.

Figure 36 shows the shaft deflection for this case at the critical speed of the model for all L/D ratios. Note the significant reduction in amplitude at the bearing mid-span as L/D increases.

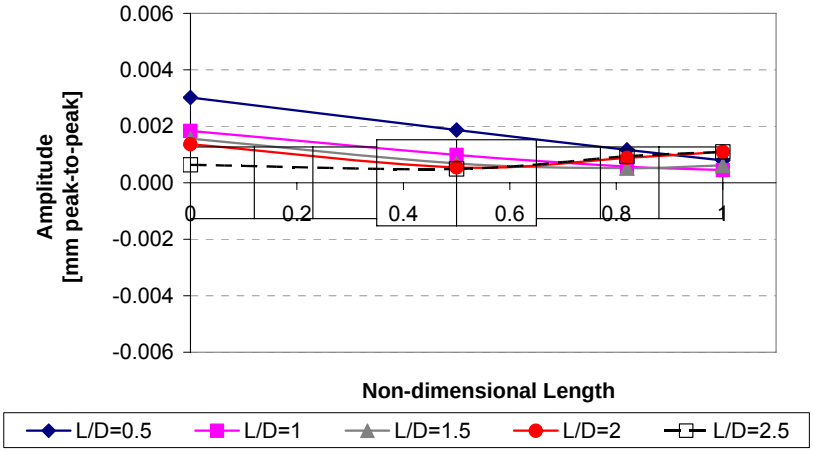

Figure 36 Shaft Deflection for Each L/D Ratio, Case B with Seal at Mid-span for the First Critical Speed (8,000 rpm)

The influence of convergent-tapered hole-pattern seal on the synchronous response of the system will be shown through Figures 37-39.

Figures 37 and 38 compare the synchronous response at bearing location and bearing mid-span for different L/D ratios, using a convergent-tapered hole-pattern seal at bearing mid-span.

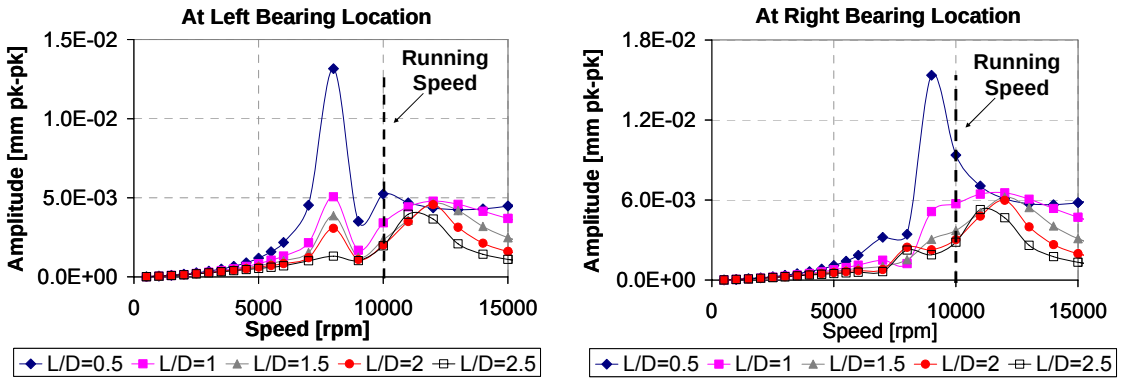

Figure 37 Synchronous Response to Unbalance at Both Bearing Locations, Case C with Seal at Mid-span

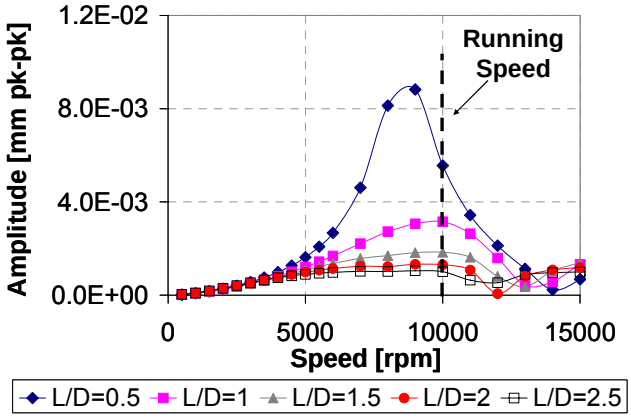

Figure 38 Synchronous Response to Unbalance at Mid-span, Case C with Seal at Mid-span

Looking at the synchronous response at both bearing locations, a significant reduction of approximately 89 percent in the critical speed response is exhibited as L/D increases from 0.5 to 2.5. At the rotor mid-span, the peak response is substantially reduced from 0.009 to 0.001 mm pk-pk (89 percent) as L/D increases.

Comparison of the synchronous response for constant clearance and convergent-tapered hole-pattern seals reveals that the critical speed is increased from 8,000 to 9,000 rpm, respectively. At rotor mid-span, convergent-tapered hole-pattern seal shows larger amplitude of vibration than that with constant clearance hole-pattern seal for all L/D ratios.

Figure 39 illustrates the shaft deflection for each L/D ratio, using convergent-tapered hole-pattern seals at the bearing mid-span. Note that the amplitude of vibration for the first critical speed (9,000 rpm) is dramatically reduced as L/D increases.

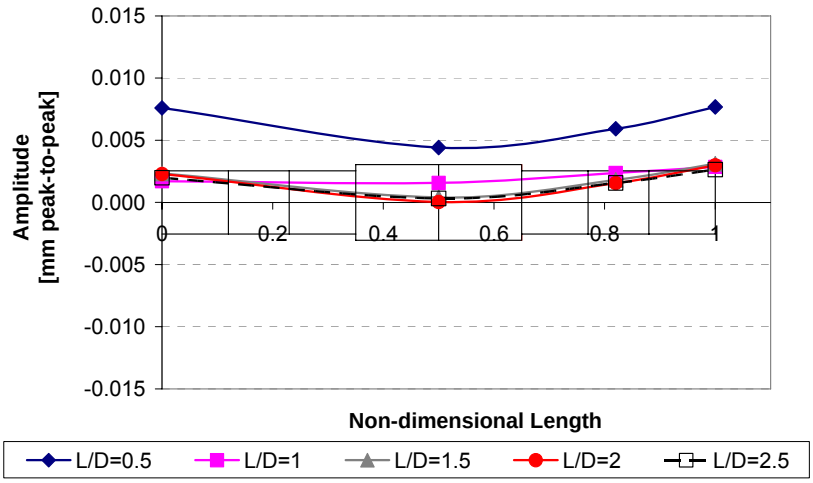

Figure 39 Shaft Deflection for Each L/D Ratio, Case C with Seal at Mid-span for the First Critical Speed (9,000 rpm)

Seal rubs is one of the concerns that inhibit the use of larger seals. In response to that, the synchronous response at both seal ends was performed for all L/D ratios and all three cases. With the seal at mid-span, the synchronous responses for all L/D ratios at both seal ends show almost not difference from the response at the seal center; that implies the seal clearance is large enough to avoid seal rubs.

In-Line Compressor with Seal at 82% of Rotor Span

Stability Analysis

Figure 40 illustrate the stability map of the system at two different configurations. For all cases, the system logarithmic decrement was predicted to be positive over all speed range, which means that the system is stable. This trend suggests that the increase of seal length while increasing the rotor length does has a significant impact in the stability of the system.

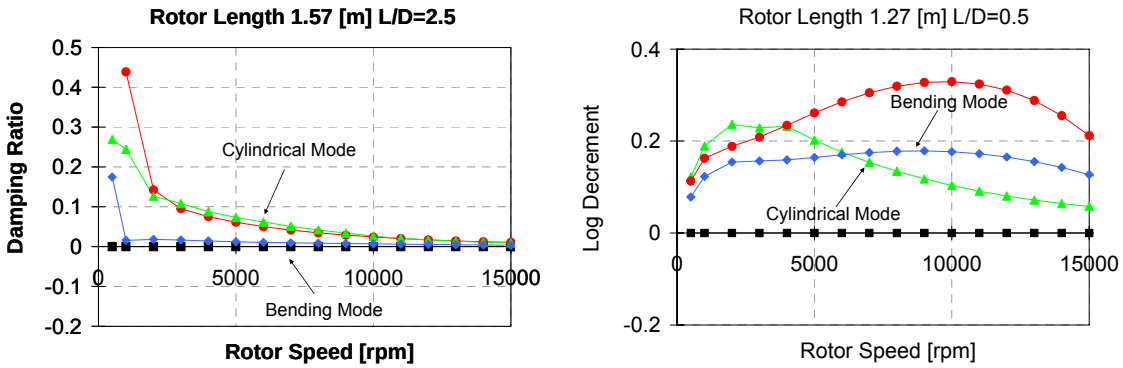

a) b)

Figure 40 Logarithmic Decrement versus Rotor Speed a) Rotor Model of 1.57 m Length with Constant Clearance Hole-Pattern Seal at 82% of Rotor Span, b) Rotor Model of 1.27 m Length with Convergent-Tapered Hole-Pattern Seal at Rotor Mid-span

Figures 41 through 43 illustrate the damped natural frequencies versus damping exponent for all L/D ratios to compare the stability for the different cases. For the three seal options A, B, and C, the system is predicted to be stable (damping exponent < 0). Note that although the system is stable for all L/D ratios, the damping exponent decays as the seal length increases, especially for case A moving from L/D=0.5 to L/D=1, and case B.

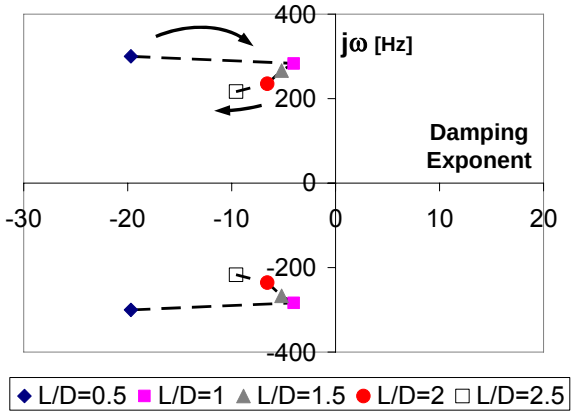

Figure 41 Damped Natural Frequency versus Damping Exponent for Case A with Seal at 82% of Rotor Span at First Critical Speed (6,000 rpm)

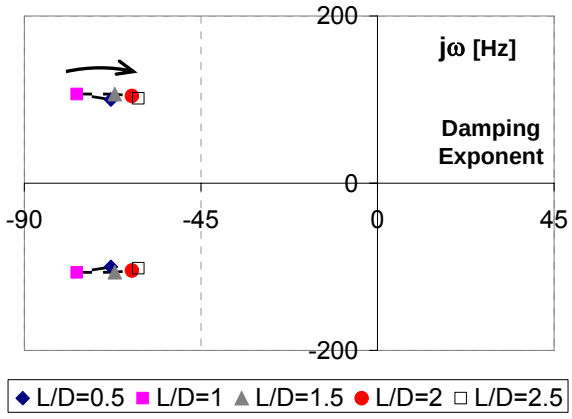

Figure 42 Damped Natural Frequency versus Damping Exponent for Case B with Seal at 82% of Rotor Span at First Critical Speed (6,000 rpm)

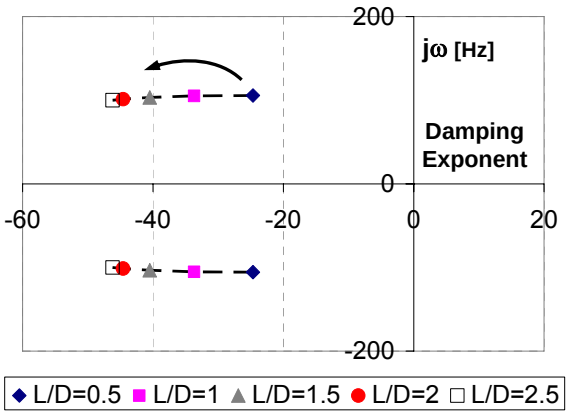

Figure 43 Damped Natural Frequency versus Damping Exponent for Case C with Seal at 82% of Rotor Span at First Critical Speed (6,000 rpm)

Synchronous Response to Unbalance

The synchronous response to unbalance of a in-line compressor model for each L/D ratio is plotted for comparison. This analysis is performed for the three cases A, B, and C.

Figures 44 and 45 show the synchronous response at bearing locations and mid-span respectively, using a constant clearance hole-pattern seal (Case A) at 82 % of rotor span.

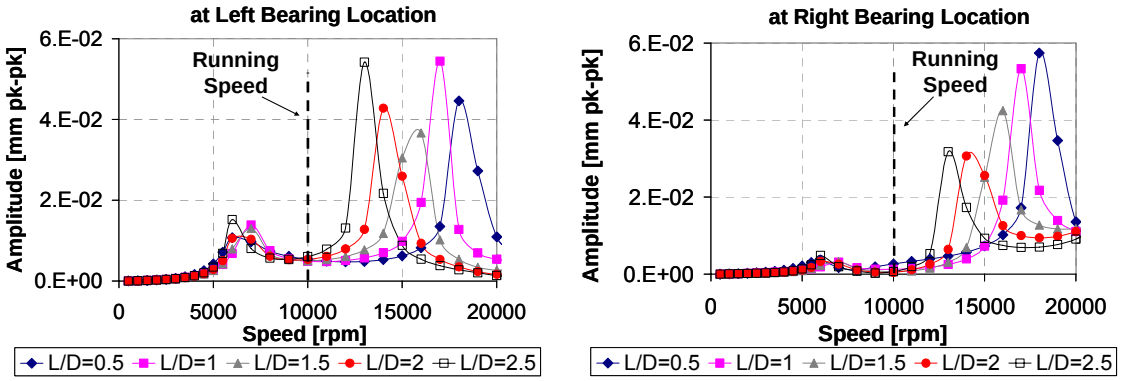

Figure 44 Synchronous Response to Unbalance at Both Bearing Locations, Case A with Seal at 82% of Rotor Span

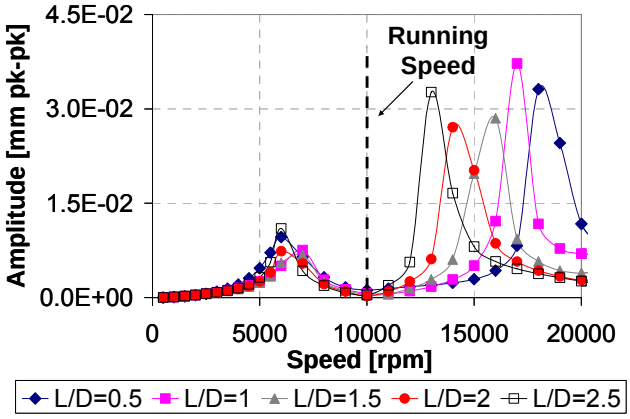

Figure 45 Synchronous Response to Unbalance at Mid-span, Case A with Seal at 82% of Rotor Span

Note from the plots that the first critical speed remains constant (6,000 rpm) and the response is slightly reduced with increasing L/D. Although the second critical speed is considerably reduced with increasing L/D, dropping from 18,000 to 13,000 rpm, it remains well above the running speed. In addition, the amplitude of vibration related to the second critical speed is reduced, especially at the right bearing location. This trend is not observed either at the left bearing location or the rotor mid-span.

Figure 46 shows the shaft deflections at both critical speeds for the rotor model using a constant clearance hole-pattern seal (Case A) at 82% bearing span. Note that the amplitude at some L/D ratios is even increased as L/D increases, compared with the initial one for both critical speed. Note that for the first mode, the seal is located near a node; therefore, it has a minimal impact on the response as L/D increases. For the first and second critical speed, the rotor shows larger amplitudes at the left bearing location than at the mid-span and right bearing, respectively, in good agreement with the synchronous response plots.

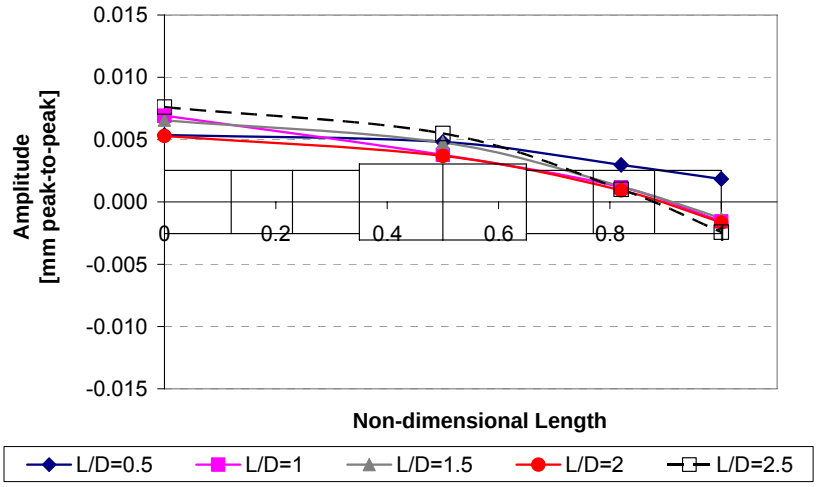

a)

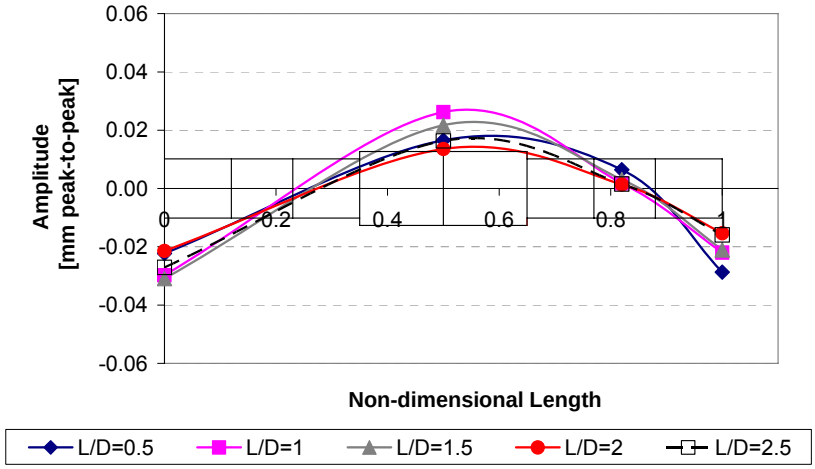

b)

Figure 46 Shaft Deflection for Each L/D, Case A with Seal at 82% of Rotor Span for a) First Critical Speeds (6,000 rpm), and b) Second Critical Speeds (18,000-13,000 rpm)

Synchronous responses for each L/D ratio for case B with seal at 82% rotor span are presented in Figures 47 and 48. Although the first critical speed (6,000 rpm) remains constant with increasing L/D, the relative peak response at bearing location and rotor mid-span is slightly reduced. However, the second critical speed is reduced from18,000 to 13,000 rpm as L/D increases from 0.5 to 2.5. Note that at the right bearing location, the amplitude of vibration related to the second critical speed is decreased from 0.057 to 0.028 mm pk-pk. However, this tendency is not exhibited at the left bearing and bearing mid-span.

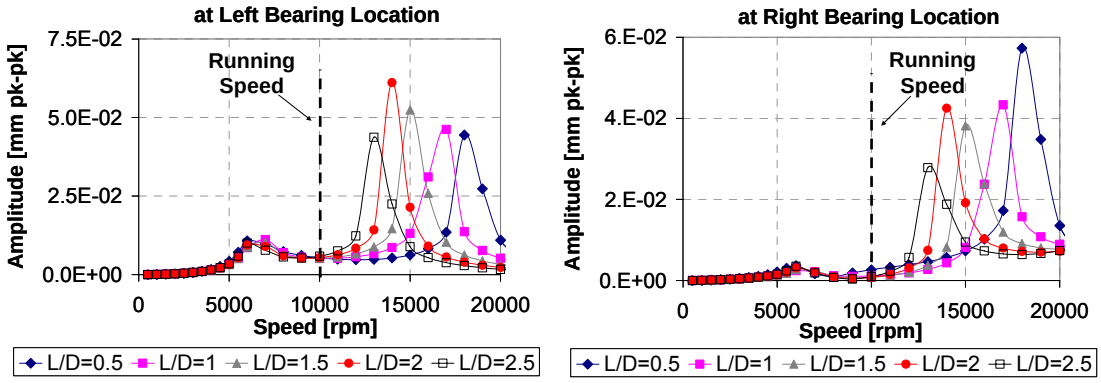

Figure 47 Synchronous Response to Unbalance at Both Bearing Locations, Case B with Seal at 82% of Rotor Span

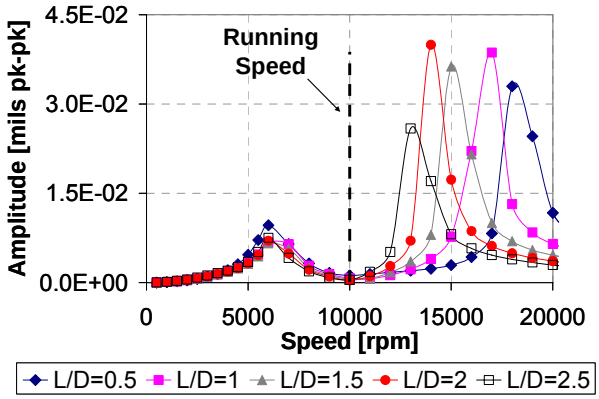

Figure 48 Synchronous Response to Unbalance at Mid-span, Case B with Seal at 82% of Rotor Span

Comparisons of synchronous response for case A and B with the seal at 82% rotor span show a slight increase in the amplitude of vibration with increasing the seal clearance.

Figure 49 shows the shaft deflections for different L/D ratios for case B. It can be seen that a slightly reduction in amplitude occurs at the first critical speed as L/D increases, since the seal is near a node. At the second critical speed (first bending mode), larger amplitudes of vibration are observed at bearing locations than at bearing mid-span.

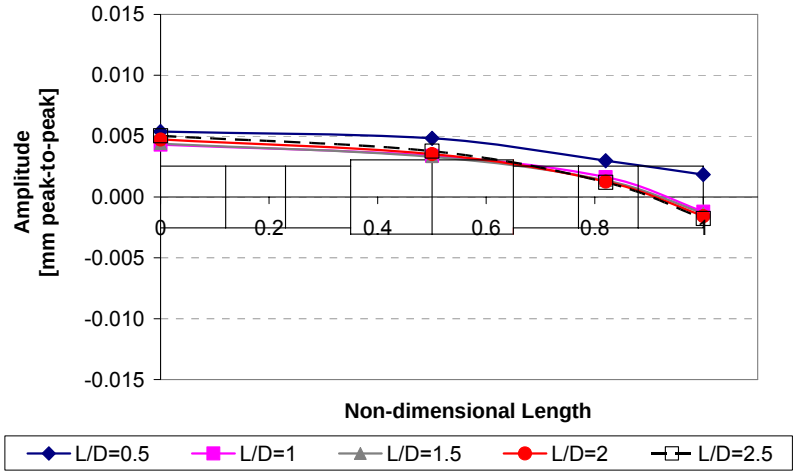

a)

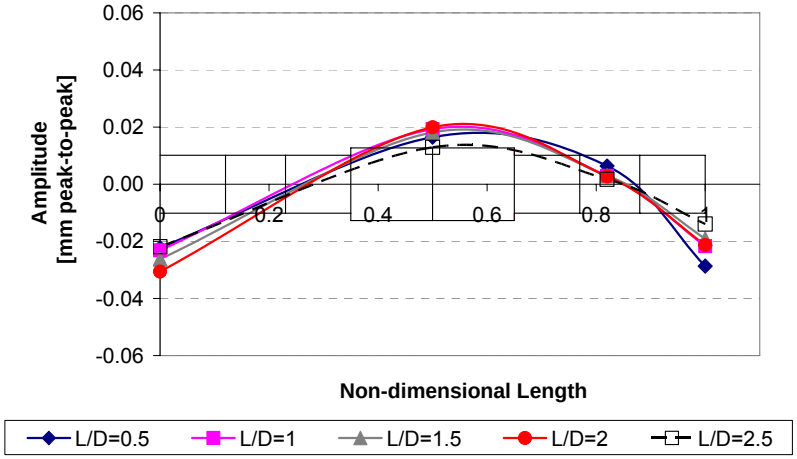

b)

Figure 49 Shaft Deflection for Each L/D, Case B with Seal at 82% of Rotor Span for a) First Critical Speeds (6,000 rpm), and b) Second Critical Speeds (18,000-13,000 rpm)

The influence of convergent-tapered hole-pattern seal located at 82% of rotor span on the synchronous response of the system will be shown through Figures 50-52.

Synchronous responses for different L/D ratios are presented in Figures 50 and 51. A small reduction in the response at the first critical speed (6,000 rpm) is observed as L/D increases from 0.5 to 2.5. In addition, the second critical speed is reduced from 18,000 to 13,000 rpm. Note that only the response at the right bearing location for the second critical speed is decreased by 40 percent as L/D increases.

In general, synchronous responses for convergent-tapered hole-pattern seal located at 82% bearing span show larger amplitudes as L/D increases than for the constant clearance hole-pattern seal at the same position.

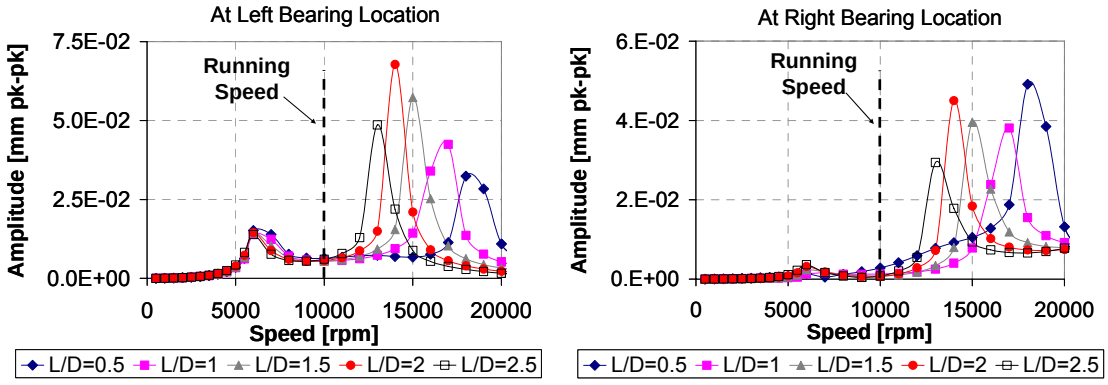

Figure 50 Synchronous Response to Unbalance at Both Bearing Locations, Case C with Seal at 82% Rotor Span

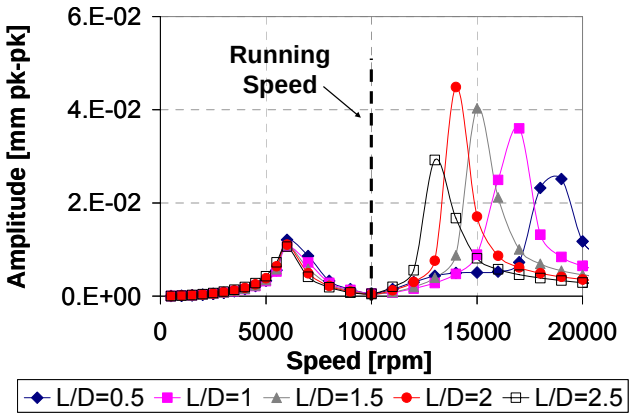

Figure 51 Synchronous Response to Unbalance at Mid-span, Case C with Seal at 82% of Rotor Span

Figure 52 illustrates the shaft deflections ratio of case C for each L/D.

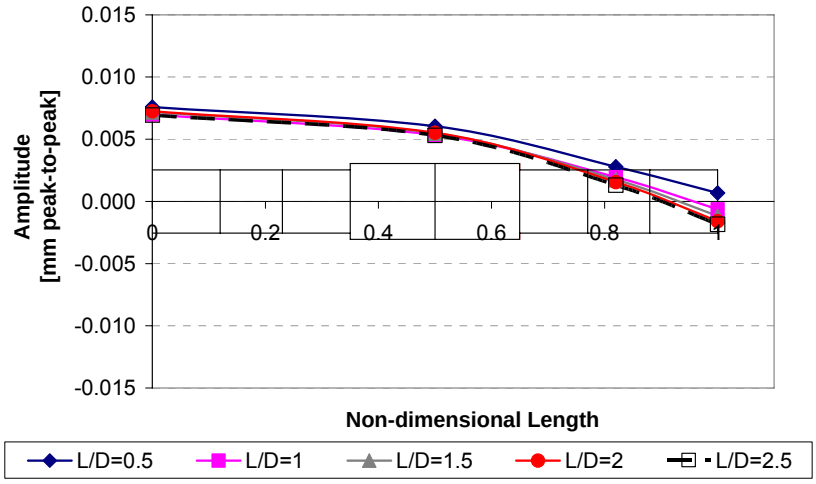

a)

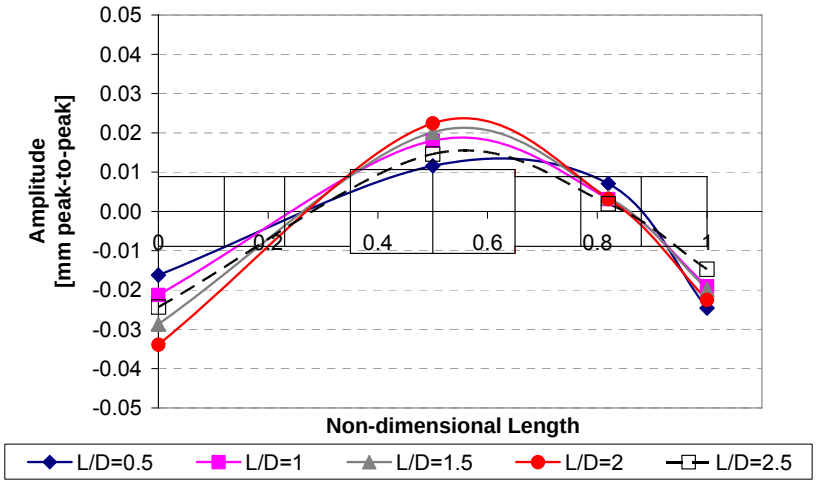

b)

Figure 52 Shaft Deflection for Each L/D Ratio, Case C with seal at 82% of Rotor Span for a) First Critical Speed (6,000 rpm), and b) Second Critical Speed (18,000-13,000 rpm)

In addition, synchronous responses at the edges of the seal were performed for all L/D ratios and all three cases to verify seal rubs. With the seal at 82% of rotor span, the synchronous responses for all L/D ratios at both seal ends show almost the exactly response at the seal center; that implies the seal clearance is large enough to avoid seal rubs.

Rotor Response to Unpressurized Seals

The synchronous response of the rotor during mechanical test (without pressure) is shown in Figures 53 and 54. Note that the first and second critical speed is reduced, while the relative response is reduced as the rotor length increases. The first critical speed is lowered from 5,000 rpm with the original rotor length to 4,500 rpm with the longer rotor. The second critical speed is 18,000 rpm with the original rotor, and is lowered to 14,000 rpm with the longer rotor. The reduction in amplitude of vibration using the longer rotor at the first critical speed is about 23 percent, and at the second critical speed is 30 percent on average, compared to the response with the original rotor length.

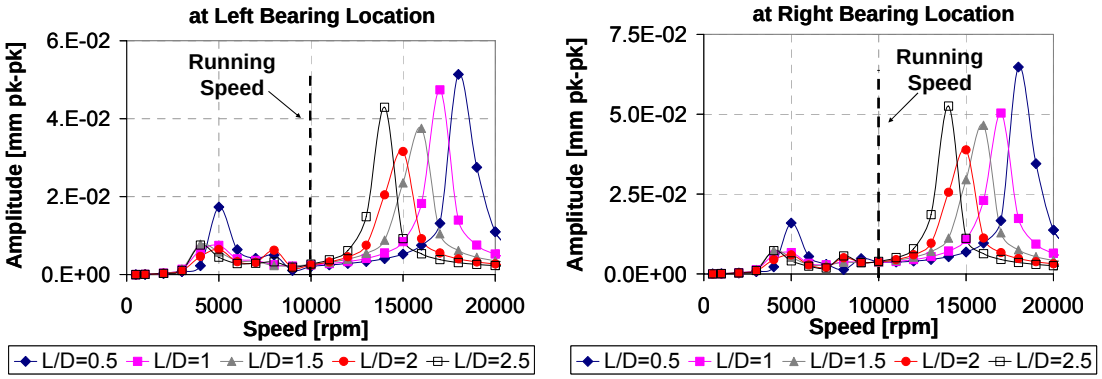

Figure 53 Synchronous Response to Unbalance at Both Bearing Locations for Different Rotor Lengths in the Absence of Pressure

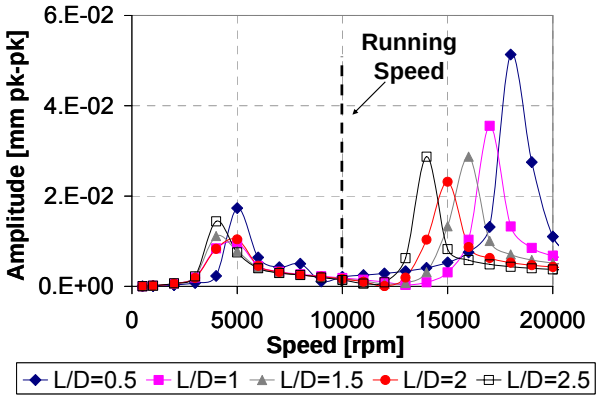

Figure 54 Synchronous Response to Unbalance at Mid-span for Different Rotor Lengths in the Absence of Pressure

SUMMARY AND CONCLUSIONS

This thesis presents the significant changes in performance and rotordynamic characteristics for a representative compressor model with longer hole-pattern seals, in particular improving leakage, stability and synchronous response for the back-to-back compressor with seal at mid-span. Predictions are compared for hole-pattern seals with L/D ratios that varies from 0.5 to 2.5. Results were obtained for back-to-back compressor with seal at mid-span and in-line compressor with seal at 82% of rotor span, considering different radial seal clearances, as well as constant clearance and convergent-tapered seal geometries.

Theoretical predictions for leakage and rotordynamic coefficients of the hole-pattern seal were calculated for the different configurations using a code based on the two-control volume model for annular gas seals developed by Kleynhans and Childs [4]. It is important to remark that this code does not include moment coefficients; parameters than can effect the results.

Results of the hole-pattern seal for all configurations indicate that the stiffness and damping coefficients increase as seal length increases. As L/D increases, predictions show higher direct stiffness values at the running speed. In addition, the results confirm the frequency-dependent model of Kleynhans and Childs. Convergent-tapered hole-pattern seals (Case A) exhibited reduced direct and larger cross-coupled stiffness compared with the constant clearance hole-pattern seal as L/D increases. In addition, the convergent-tapered hole-pattern seals (Case C) show less damping than the constant clearance hole-pattern seals as L/D increases. The increase of radial clearance as L/D increases for constant clearance seals (Case B) had an effect on the rotordynamic coefficients; the stiffness and especially damping is reduced, compared to that with constant clearance as L/D increases.

Predictions for leakage flow rate exhibit a significant reduction of approximately 47 percent as L/D increases from 0.5 to 2.5, for both constant clearance and convergent-tapered hole-pattern seals, showing that seal length is an important factor to minimize leakage. Results for constant clearance hole-pattern seals show an average of 35 percent less leakage than the convergent-tapered hole-pattern seals for each L/D

ratio. Cases B and C maintain constant a leakage flow rate value of 3.6 kg/s, while increasing L/D, the same leakage as Case A for L/D ratio of 0.5.

Results for static stiffness show a significant reduction with increasing L/D ratios for cases A and B. However for convergent-tapered seals, the reduction in static stiffness as L/D increases from 1 to 2.5 is just about 16 percent. In addition, convergent-tapered seal exhibits larger static stiffness values, compared to constant clearance seals.

For back-to back compressor with the seal located at mid-span, the influence of increasing L/D on stability and synchronous response results is significant. The linear stability analysis of the rotor model predicts a critical speed at 8,000 rpm for all L/D, associated with a cylindrical bending mode. For all cases, the system is predicted to be stable for all speeds, and all L/D ratios. In fact, comparisons of damping exponents for each L/D ratio indicate that the cylindrical bending mode becomes more stable with increasing L/D ratio for the three cases A, B, and C.

The most impressive result for is the dramatic reduction in synchronous amplitude as L/D increases for the constant clearance and convergent-tapered hole-pattern seal. For case A, the synchronous response at the bearing mid-span shows a critical speed at 8,000 rpm for all L/D ratios. Results show a substantial reduction of 85 percent in the peak response as seal length increases from 0.5 to 2.5. In addition, the response at bearing location is significantly reduced. Increasing the radial seal clearance while L/D increases, slightly increases the synchronous response of the model compared with constant clearance. For convergent-tapered hole-pattern seals, the synchronous response at the bearing mid-span shows not only a higher critical speed (9,000 rpm) for all L/D ratios, but also a larger reduction (89 percent) in peak response with increasing seal length, compared to that for constant clearance hole-pattern seals. However, the magnitude of the peak response is larger for convergent-tapered hole-pattern seals than for constant clearance hole-pattern seals, for all L/D ratios. Synchronous response at seal ends for all cases indicates that seals do not rub.

In summary, results show that long hole-pattern seals located at the mid-span are a potential application to improve leakage performance and synchronous response of back-to-back compressors. Results indicate that the increase of seal's stiffness and damping is significant to not only keep the critical speed constant, while simultaneously

the leakage is reduced, the stability improved and the peak response remarkable reduced.

On the other hand, for in-line compressor with the seal at 82% of rotor span, the linear stability analysis predicts two critical speeds occurring at 6,000 and 18,000 rpm respectively. The first critical speed corresponds to the rotor conical mode, showing larger amplitudes at the left bearing location. The second critical speed is associated with the rotor first bending mode. Both modes are predicted to be stable (log dec > 0) for all speed and L/D ratios. However, the conical mode becomes less stable with increasing L/D, especially for cases A and B.

For all cases, the peak response at the mid-span relative to the first critical speed is slightly reduced as L/D increases since the seal is near a node, while the response at the second critical speed is generally increased. Note that although the second critical speed is reduced as L/D increases, dropping from 18,000 to 13,000 rpm, it remains well above the running speed. Some other rotors might have a second critical speed that drops into the running speed as L/D increases; however, that was not the case for this model. Also, the amplitude of vibration at both critical speeds is larger with increasing of radial clearance as L/D increases, compared to that for constant radial clearance. Seal rubs is not a concern for this case. In conclusion, for in-line compressors the increment of seal length does not have any impact of interest.

Synchronous response of the rotor during mechanical test (without pressure) shows two critical speeds occurring at 5,000 and 18,000 rpm respectively. As seal length increases, the synchronous response at both critical speeds are reduced. However, the second critical speed is reduced from 18,000 rpm to 14,000 rpm.

REFERENCES

[1] Childs, D., “Turbomachinery Rotordynamics – Phenomena, Modeling and Analysis,” John Wiley & Sons, 1993.

[2] Fowlie, D. W., and Miles, D. D., 1975, “Vibration Problems with High Pressure Centrifugal Compressors,” ASME Paper Number 75-Pet-28, Petroleum Engineering Conference, Tulsa, Oklahoma.

[3] Fulton, J. W., 1984, “The Decision to Full Load Test a High Pressure Centrifugal Compressor in its Module Prior to Tow-out,” Institution of Mechanical Engineers, **I**, pp. 133-138.

[4] Sood, V. K., 1979, “Design and Full Load Testing of a High Pressure Centrifugal Natural Gas Injection Compressor,” Proceedings of the Eighth Turbomachinery Symposium, Turbomachinery Laboratory, Texas A&M University, College Station, Texas, pp. 35-42.

[5] Kleynhans, G., and Childs, D.,1997, “The Acoustic Influence of Cell Depth on the Rotordynamic Characteristics of Smooth-Rotor/Honeycomb-Stator Annular Gas Seals,” ASME Trans., Journal of Engineering for Gas Turbines and Power, October 1997, **119**, No. 4, pp. 949-957.

[6] Dawson, M. P., 2000, ‘‘A Comparison of the Static and Dynamic Characteristics of Straight-Bore and Convergent Tapered-Bore Honeycomb Annular Gas Seals,’’ M.S. Thesis, Texas A&M University, College Station.

[7] Holt, C., and Childs, D., 2002, “Theory Versus Experiment Results for the Dynamic Impedances of Two Hole-Pattern Annular Gas Seals,” ASME Journal of Tribology, **24**, pp. 137-143.

[8] Weatherwax, M., and Childs, D., 2002, “The Influence of Eccentricity Effects on the Rotordynamic Coefficients of a High-Pressure Honeycomb Gas Seal, Measurements Versus Predictions,” ASME Paper 2002-TRIB-207.

[9] Wade, J., 2001, “Test Versus Predictions for Rotordynamic Coefficients and Leakage Rates of Hole-Pattern Gas Seals at Two Clearances in Choked and Unchoked Conditions,” M.S. Thesis, Department of Mechanical Engineering, Texas A&M University, College Station.

[10] Childs, D. and Wade, J., 2004, “Rotordynamic-Coefficient and Leakage Characteristics for Hole-Pattern-Stator Annular Gas Seals — Measurements Versus Predictions,“ ASME Transactions, Journal of Tribology, **126**, p. 326-333.

[11] Sprowl, T., 2003, “A Study of the Effects of Inlet Preswirl on the Dynamic Coefficients of a Straight-Bore Honeycomb Gas Damper Seal,” M.S. Thesis, Department of Mechanical Engineering, Texas A&M University.

[12] Childs, D., and Moyer, D., 1985, “Vibration Characteristics of the HPOTP (High Pressure Oxygen Turbopump) of the SSME (Space Shuttle Main Engine),” ASME Journal of Engineering for Gas Turbine and Power, **107**, pp. 152-159.

[13] Zeidan, F., Perez, R., and Stephenson, M., 1993, “The Use of Honeycomb Seals in Stabilizing Two Centrifugal Compressors,” Proceedings of the Twenty-second Turbomachinery Symposium, Turbomachinery Laboratory, Texas A&M University, College Station, Texas, pp. 3-15.

[14] Sorokes, J., Kuzdal, M., Sandberg, M., and Colby, G., 1994, “Recent Experience in Full Load Full Pressure Shop Testing of a High Pressure Gas Injection Centrifugal Compressor,” Proceedings of the Twenty-third Turbomachinery Symposium, Turbomachinery Laboratory, Texas A&M University, College Station, Texas, pp. 3-17.

[15] Armstrong, J., and Perricone, F., 1996, “Turbine Instability Solution-Honeycomb Seals,” Proceedings of the Twenty-fifth Turbomachinery Symposium, Turbomachinery Laboratory, Texas A&M University, College Station, Texas, pp. 47-56.

[16] Moore, J., Walker, S., and Kuzdal, M., 2002, “Rotordynamic Stability Measurements During Full Load Testing of a 6000 psi Reinjection Centrifugal Compressor,” Proceedings of the Thirty-first Turbomachinery Symposium, Turbomachinery Laboratory, Texas A&M University, pp. 29-38.

[17] Fleming, D., 1979, “Stiffness of Straight and Tapered Annular Gas Seals,” ASME Journal of Lubrication Technology, **101**, No. 3, pp. 349-355.

VITA

Name: Margarita Rodrigues Rodrigues

Education: BS. Mechanical Engineering, Universidad Simón Bolívar, March 2004
MS. Mechanical Engineering, Texas A&M University, December 2006

Email: margarita@tamu.edu

Address: 5510 S. Rice Ave. Apt# 1431
Houston, Texas 77081